Clim. Past, 20, 363–392, 2024
https://doi.org/10.5194/cp-20-363-2024

Climate of the Past
Open Access
EGU

A global compilation of diatom silica oxygen isotope records from lake sediment – trends and implications for climate reconstruction

Philip Meister[1,★], Anne Alexandre[2], Hannah Bailey[3], Philip Barker[4], Boris K. Biskaborn[1], Ellie Broadman[5], Rosine Cartier[2,6], Bernhard Chapligin[1], Martine Couapel[2], Jonathan R. Dean[7], Bernhard Diekmann[1,8], Poppy Harding[9,17], Andrew C. G. Henderson[10], Armand Hernandez[11], Ulrike Herzschuh[1,12,13], Svetlana S. Kostrova[1], Jack Lacey[14], Melanie J. Leng[14,15], Andreas Lücke[16], Anson W. Mackay[17], Eniko Katalin Magyari[18], Biljana Narancic[19,1], Cécile Porchier[20], Gunhild Rosqvist[21], Aldo Shemesh[22], Corinne Sonzogni[2], George E. A. Swann[23], Florence Sylvestre[2], and Hanno Meyer[1,★]

[1]Alfred Wegener Institute Helmholtz Centre for Polar and Marine Research, Polar Terrestrial Environmental Systems, Potsdam, 14473, Germany
[2]Aix Marseille University, CNRS, IRD, INRAE, Coll France, CEREGE, Aix-en-Provence, 13545, France
[3]Water, Energy and Environmental Engineering Research Unit, University of Oulu, P.O. Box 8000, Oulu, Finland
[4]Lancaster Environment Centre, Lancaster University, Lancaster, LA1 4YQ, UK
[5]Laboratory of Tree-Ring Research, University of Arizona, Tucson, Arizona, AZ 85721-0045, USA
[6]Department of Geology, Lund University, Lund, 223 62, Sweden
[7]Department of Geography, Geology & Environment, University of Hull, Hull, HU6 7RX, UK
[8]Institut für Geowissenschaften, Universität Potsdam, Potsdam, 14476, Germany
[9]Geography, Environment & Planning, University of Hertfordshire, Hatfield, AL10 9AB, UK
[10]School of Geography, Politics and Sociology, Newcastle University, Newcastle upon Tyne, NE1 7RU, UK
[11]GRICA Group, Centro Interdisciplinar de Química e Bioloxía (CICA), Faculty of Sciences, Universidade da Coruña, A Coruña, 15008, Spain
[12]Institute of Environmental Science and Geography, University of Potsdam, 14476, Germany
[13]Institute of Biochemistry and Biology, University of Potsdam, Potsdam, 14476, Germany
[14]National Environmental Isotope Facility, Isotope Geosciences Facility, British Geological Survey, Keyworth, Nottingham, NG12 5GG, UK
[15]Centre for Environmental Geochemistry, School of Biosciences, University of Nottingham, Sutton Bonington, LE12 5RD, UK
[16]Institute of Bio- and Geosciences, Agrosphere Institute IBG-3, Forschungszentrum Jülich GmbH, Jülich, 52428, Germany
[17]Environmental Change Research Centre, Department of Geography, University College London, London, WC1E 6BT, UK
[18]Department of Environmental and Landscape Geography, MTA-MTM-ELTE Research Group for Paleontology, Eötvös Loránd University, Budapest, 1117, Hungary
[19]Laboratoire de Paléoécologie Aquatique, Centre d'Études nordiques & Département de géographie, Université Laval, Laval, G1V 0A6, Canada
[20]Department of Geography, University College London, London, WC1E 6BT, UK
[21]Department of Physical Geography, Stockholm University, Stockholm, 106 91, Sweden
[22]Department of Earth and Planetary Sciences, the Weizmann Institute of Science, Rehovot, 76100, Israel
[23]School of Geography, University of Nottingham, University Park, Nottingham, NG7 2RD, UK
★These authors contributed equally to this work.

Correspondence: Hanno Meyer (hanno.meyer@awi.de)

Published by Copernicus Publications on behalf of the European Geosciences Union.

Received: 16 December 2022 – Discussion started: 24 January 2023
Revised: 1 November 2023 – Accepted: 9 January 2024 – Published: 26 February 2024

Abstract. Oxygen isotopes in biogenic silica ($\delta^{18}O_{BSi}$) from lake sediments allow for quantitative reconstruction of past hydroclimate and proxy-model comparison in terrestrial environments. The signals of individual records have been attributed to different factors, such as air temperature (T_{air}), atmospheric circulation patterns, hydrological changes, and lake evaporation. While every lake has its own local set of drivers of $\delta^{18}O$ variability, here we explore the extent to which regional or even global signals emerge from a series of paleoenvironmental records. This study provides a comprehensive compilation and combined statistical evaluation of the existing lake sediment $\delta^{18}O_{BSi}$ records, largely missing in other summary publications (i.e. PAGES network). For this purpose, we have identified and compiled 71 down-core records published to date and complemented these datasets with additional lake basin parameters (e.g. lake water residence time and catchment size) to best characterize the signal properties. Records feature widely different temporal coverage and resolution, ranging from decadal-scale records covering the past 150 years to records with multi-millennial-scale resolution spanning glacial–interglacial cycles. The best coverage in number of records ($N = 37$) and data points ($N = 2112$) is available for Northern Hemispheric (NH) extratropical regions throughout the Holocene (roughly corresponding to Marine Isotope Stage 1; MIS 1). To address the different variabilities and temporal offsets, records were brought to a common temporal resolution by binning and subsequently filtered for hydrologically open lakes with lake water residence times < 100 years. For mid- to high-latitude ($> 45°$ N) lakes, we find common $\delta^{18}O_{BSi}$ patterns among the lake records during both the Holocene and Common Era (CE). These include maxima and minima corresponding to known climate episodes, such as the Holocene Thermal Maximum (HTM), Neoglacial Cooling, Medieval Climate Anomaly (MCA) and the Little Ice Age (LIA). These patterns are in line with long-term air temperature changes supported by previously published climate reconstructions from other archives, as well as Holocene summer insolation changes. In conclusion, oxygen isotope records from NH extratropical lake sediments feature a common climate signal at centennial (for CE) and millennial (for Holocene) timescales despite stemming from different lakes in different geographic locations and hence constitute a valuable proxy for past climate reconstructions.

1 Introduction

1.1 Scientific background

Oxygen isotopes are ubiquitous within the global water cycle and are among the best (hydro)climate proxies worldwide as a result of their potential quantitative interpretability. The most abundant isotope ^{16}O and the rarer isotope ^{18}O are subject to fractionation during water-phase transformation and transport processes (Fig. 1). As a result, the relative abundance of these isotopes varies across space, time, and reservoirs. The IAEA's standard Vienna Standard Mean Ocean Water (VSMOW) serves as a baseline, closely resembling the isotopic composition of modern seawater. Relative abundance of ^{18}O with regard to ^{16}O is expressed relative to the VSMOW standard as $\delta^{18}O$ and given in units of per mill.

Measuring $\delta^{18}O$ in water, vapour, snow, and ice allows for quantifying hydroclimatic processes in the global water cycle and has been used to this end for many decades (Dansgaard, 1964; Konecky et al., 2020). In addition to its use in present-day hydrology, $\delta^{18}O$ in environmental archives also serves as a powerful proxy for past hydrology and, in turn, climate. As such, $\delta^{18}O$ is a crucial and quantitative tool for both reconstructions of past climate and for comparison of proxy data to climate model outputs.

Oxygen isotope records are available from different paleoenvironmental archives, e.g. in glaciers and ice sheets (Andersen et al., 2004), permafrost (Meyer et al., 2015b), and marine (Spielhagen and Mackensen, 2021) and lacustrine (Leng, 2006) environments, as well as different materials, such as carbonates (Kwiecien et al., 2014), silicates (Leng, 2006), biomarkers (Lasher et al., 2017), cellulose (Wolfe et al., 2007), glacier ice (Andersen et al., 2004), and ground ice (Opel et al., 2017). Therefore, oxygen isotopes offer the possibility for directly comparing data from different paleoenvironmental archives.

The predictability of isotope fractionation processes in the water cycle due to clear physical constraints allows for using $\delta^{18}O$ not only as a quantitative tool for past (hydro)climate reconstructions but also for implementing $\delta^{18}O$ in global climate models (e.g. Danek et al., 2021). However, challenges persist in understanding and comparing data and model outputs, partly due to complex signal formation in environmental archives (Danek et al., 2021).

Lake sediments are prominent and widespread archives in terrestrial environments (Leng, 2006; Biskaborn et al., 2016; Subetto et al., 2017). Like glaciers and ice caps, lakes may record the isotopic signature of past precipitation (Shemesh et al., 2001a). The signal formation in lakes, however, is fundamentally different from that in glaciers and ice caps, with

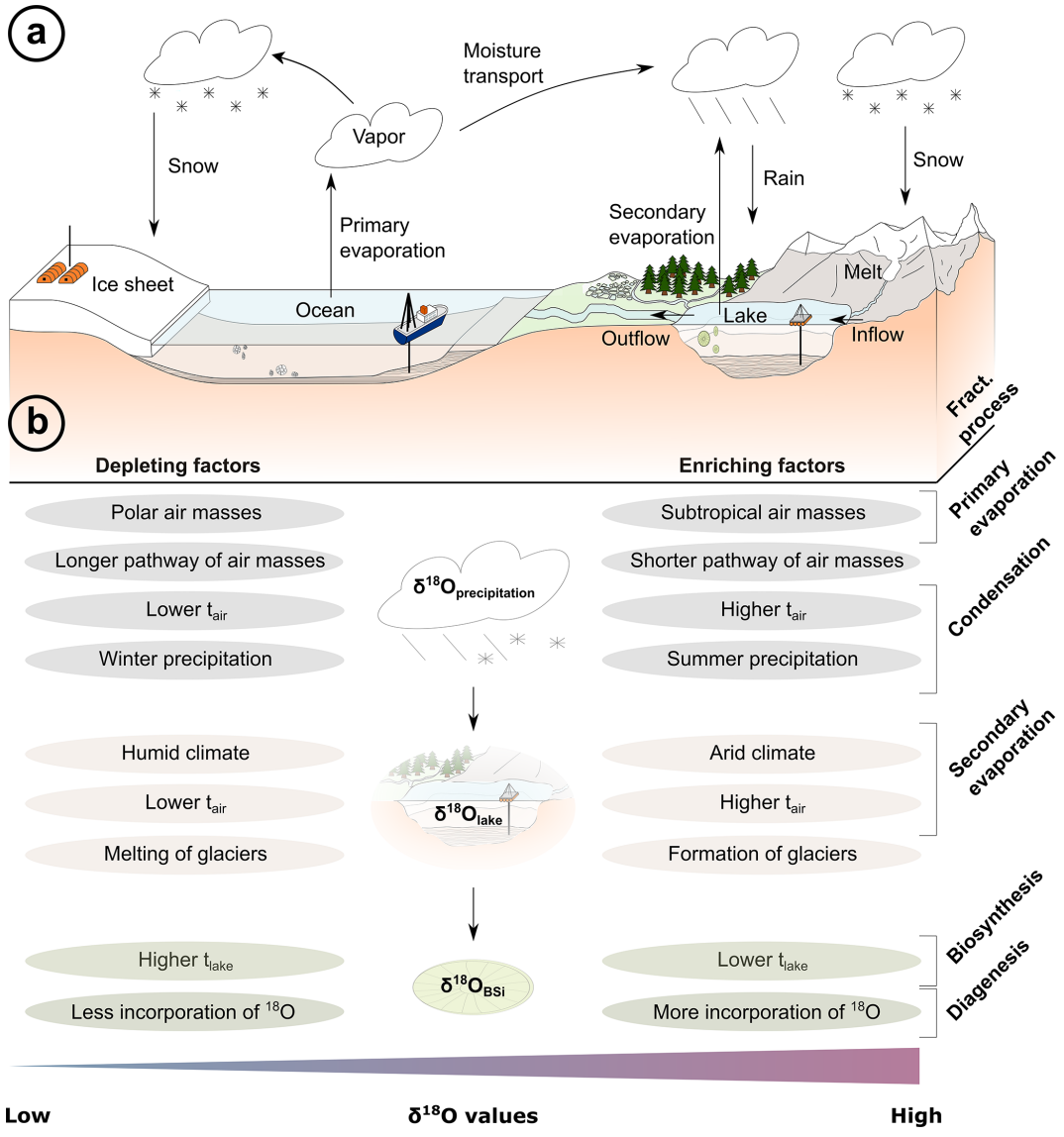

Figure 1. Schematic overview of select reservoirs and processes within the global water cycle influencing the $\delta^{18}O_{BSi}$ signal of records. **(a)** Overview of the global water cycle with reservoirs and processes. **(b)** Depleting and enriching factors influencing $\delta^{18}O$ values in precipitation, lake water, and biogenic silica. Corresponding fractionation processes are indicated on the right-hand side.

the lake waterbody acting as a buffer of the enclosed (hydro)climate signal, influenced by factors such as catchment hydrology, lake ontogeny, and sediment accumulation rates (Bittner et al., 2021). While biogenic silica is also found in phytoliths, sponge spicules, and chrysophytes, this study focuses exclusively on diatoms. Diatoms are microscopic algae that synthesize their frustules from lake water and the silica dissolved therein, thereby preserving the isotope signal of past lake water. The oxygen isotope composition of the biogenic silica of diatom frustules ($\delta^{18}O_{BSi}$) buried in lake sediment therefore provides valuable insight on past lake water and, in turn, precipitation.

Naturally, the interplay of hydrological and sedimentological processes limits the time span and resolution over which environmental information can be obtained from a lake system, and this varies from lake to lake. Most commonly, $\delta^{18}O_{BSi}$ has been applied to lake sediments devoid of carbonates. These lakes are especially common in high-altitude and high-latitude regions (Leng and Barker, 2006).

1.2 Controls on $\delta^{18}O_{BSi}$

Due to the complex signal formation in $\delta^{18}O_{BSi}$ records, most authors refer to a combination of factors for interpreting any given individual record. A schematic overview of some of the main processes is provided in Fig. 1 and

by Leng and Barker (2006). Lake water temperature (T_{lake}) imparts a direct effect on $\delta^{18}O_{BSi}$ due to temperature-dependent fractionation during biosynthesis of biogenic silica. Temperature-dependent fractionation coefficients were initially determined for marine environments (Leclerc and Labeyrie, 1987; Matheney and Knauth, 1989) and later estimated for lacustrine sediments as ca. -0.2 ‰ per °C during biosynthesis (Dodd and Sharp, 2010; Moschen et al., 2005). However, the applicability of these calibrations to sedimentary records is debated due to possible disequilibrium between diatom frustules and lake water, as well as taphonomic and diagenetic processes (Leng and Barker, 2006; Ryves et al., 2020; Smith et al., 2016; Tyler et al., 2017).

More commonly, changes in $\delta^{18}O_{BSi}$ are attributed to $\delta^{18}O$ changes in lake water ($\delta^{18}O_{lake}$) and thereby, with the lake as a buffer, to the isotopic composition of precipitation ($\delta^{18}O_{precipitation}$). Locally, $\delta^{18}O_{precipitation}$ is primarily influenced by air temperature (T_{air}) with a fractionation of 0.7 ‰ per °C on global average (Dansgaard, 1964). On a broader scale, parameters such as precipitation moisture source and air mass trajectory patterns are important, and changes in $\delta^{18}O_{BSi}$ records may be indicative of shifting atmospheric circulation patterns (Bailey et al., 2015) that affect the local ratio of precipitation to evaporation (P/E). The parameter P/E refers to the balance between the amount of precipitation and evaporation within a lake's catchment. Typically, water loss through evaporation leads to higher $\delta^{18}O_{lake}$ values due to evaporative enrichment and therefore higher $\delta^{18}O_{BSi}$. Precipitation amount and seasonality (e.g. rain vs. snow) will also strongly impact the isotope signal of the lake water (Meyer et al., 2022). Disentangling the effects of precipitation and evaporation in $\delta^{18}O_{BSi}$ records is thus a major challenge, and therefore some authors commonly refer to P/E changes in conjunction with other factors (Hernandez et al., 2013; Rosqvist et al., 2013; Broadman et al., 2020a).

Shemesh et al. (2001a) have attributed the $\delta^{18}O_{BSi}$ signal changes of Lake 850 in Swedish Lapland to different contributions of main source regions of precipitation, namely the Atlantic and Arctic oceans. Indeed, for this location, changes in atmospheric circulation patterns imply changes in both T_{air} and humidity.

Additionally, $\delta^{18}O_{precipitation}$ may also be linked to shifts in the seasonality of precipitation (Swann et al., 2010; Kostrova et al., 2016; Harding et al., 2020), which is linked to T_{air} change, but also atmospheric circulation patterns (Shemesh et al., 2001a; Jones et al., 2004; Leng et al., 2005; Rosqvist et al., 2013) and, on longer timescales, insolation (Swann et al., 2010; Kostrova et al., 2019, 2021). T_{air} as often inferred from $\delta^{18}O_{BSi}$ can, therefore, be a parameter with local, regional, and global significance.

Insolation is not an environmental parameter that can be inferred from $\delta^{18}O_{BSi}$ records. It is, however, commonly used as an explanatory variable and underlying driver of Holocene climate change. Insolation can be calculated for any given place throughout time (Laskar et al. 2004), which allows for direct comparison with $\delta^{18}O_{BSi}$ time series. Insolation primarily influences T_{air} and, indirectly, the P/E balance and atmospheric circulation patterns.

Moreover, hydrological processes within a lake's catchment may substantially impact $\delta^{18}O_{lake}$ and hence $\delta^{18}O_{BSi}$. Some of these processes are closely linked to climate and precipitation patterns described above. Most notable are variations in the amount of snowmelt (Mackay et al., 2013; Rosqvist et al., 2013; Meyer et al., 2022) and glacial influx (Meyer et al., 2015a) to a lake. Glaciers or snow fields in the hinterland may provide more melt (with lower or depleted $\delta^{18}O$) in warm phases and may counter the influence of warming on $\delta^{18}O_{precipitation}$ (Meyer et al., 2015a).

Other hydrological processes, however, are only indirectly linked to climate. These include the formation and closure of outflows to the lake which change the lake's hydrological setting (Hernandez et al., 2008; Vyse et al., 2020; Bittner et al., 2021). Associated changes in the mass balance of a lake, and thus the P/E-balance, may lead to a different $\delta^{18}O_{BSi}$ signal. Within the lake itself, long-term diagenetic effects on diatoms include recrystallization and incorporation of heavier ^{18}O from silanol bonds into the Si–O–Si crystal lattice – a process that may increase the original $\delta^{18}O_{BSi}$ signal (cf. Akse et al., 2022; Fig. 1). However, despite notable recrystallization, Chapligin et al. (2012b) found no significant diagenetic effect in records spanning the past 250 kyr.

To interpret a given $\delta^{18}O_{BSi}$ record, information about the present hydrology is thus important as it provides insight on which processes influence $\delta^{18}O_{lake}$ and, in turn, $\delta^{18}O_{BSi}$. Naturally, as the hydrology of a given lake can only offer snapshots of present-day constraints, caution has to be applied when extrapolating these into the past. The isotopic composition of three components is of interest for assessing the signal properties of $\delta^{18}O_{BSi}$ records: (1) $\delta^{18}O_{lake}$, (2) $\delta^{18}O$ of inflows to the lake, and (3) $\delta^{18}O_{precipitation}$. The lake water composition can provide insight on whether lake water is isotopically homogenous, both spatially and at different depths of the lake basin. Offsets of $\delta^{18}O_{lake}$ from the Local Meteoric Water Line (LMWL) give hints as to whether or not lake evaporation may have had a significant effect on lake water isotopic composition. $\delta^{18}O_{lake}$ can also be used in conjunction with T_{lake} and the most recent $\delta^{18}O_{BSi}$ value for testing the temperature-dependent fractionation and, in turn, the applicability of the proxy for paleoclimate reconstructions (cf. Meyer et al. 2015a). Complementary isotope measurements of lake inflows (i.e. rivers, streams) provide further information on specific hydrological constraints. For larger lakes and catchments, the different inflows and their effect on the lake's isotopic mass balance have been used for inferring changing hydrology or precipitation regimes in different parts of the catchment (e.g. Mackay et al. 2011). Additionally, while $\delta^{18}O_{precipitation}$ data are critical for constraining modern climate–isotope relationships, they are often not available and only few monitoring studies of $\delta^{18}O_{precipitation}$ and $\delta^{18}O_{lake}$ in combination with $\delta^{18}O_{BSi}$ exist (Kostrova

et al., 2019; Hernandez et al., 2010). A possible alternative can be derived from the GNIP database (IAEA/WMO, 2022) and spatial interpolations thereof, e.g. the Online Isotopes in Precipitation Calculator (Bowen, 2022).

1.3 Sample preparation and measurement

Extracting pure diatom valves (frustules) from lake sediments is a complex process and depends on a sufficiently high diatom concentration in the sediment. Various cleaning procedures for diatom extraction exist, which are mainly based on the use of H_2O_2 for removing organic matter from the sediment and HCl for the removal of carbonate (Chapligin et al., 2012a). Detrital components are often separated through centrifugation in heavy liquid solution (i.e. sodium polytungstate) at variable specific densities (Morley et al., 2004; Chapligin et al., 2012a). Different procedures in sample preparation, i.e. different temperatures, may result in offsets of measured $\delta^{18}O_{BSi}$ (Swann et al., 2010; Chapligin et al., 2012b; Tyler et al., 2017). Impurities due to incomplete removal of detrital components may also affect the measured $\delta^{18}O_{BSi}$ (Lamb et al., 2005; Chapligin et al., 2012b). To account for this, the purity of samples is usually assessed prior to measurement by visual inspection or direct measurement of the amount of contaminants of a given sample (Bailey et al., 2018; Broadman et al., 2020a). Fewer studies determine the isotopic composition of detrital contaminants to apply a correction to the measured $\delta^{18}O_{BSi}$ values (Brewer et al., 2008; Mackay et al., 2011; Wilson et al., 2014a; Bittner et al., 2021; Kostrova et al., 2021). Consequently, caution has to be applied when comparing absolute values of different individual $\delta^{18}O_{BSi}$ records, as offsets between individual records may result from both different preparation and measurement techniques, as well as regional differences in $\delta^{18}O_{lake}$. The potential and challenges associated with data stemming from different preparation and measurement techniques have already been addressed (Chapligin et al., 2011; Mackay et al., 2011).

1.4 Aim of this work

A comprehensive compilation and assessment of the lacustrine $\delta^{18}O_{BSi}$ records published to date is missing. Due to the crucial role of lake and catchment hydrology in signal formation, such a compilation needs to include individual lake basin parameters, such as lake volume and water residence time (t_{res}), to provide reliable constraints for interpreting and comparing the individual records. Proxy data compilations have already addressed a lack of standardized metadata, data availability, and data uniformity of paleo-data (Pfalz et al., 2021). However, such compilations generally do not include $\delta^{18}O_{BSi}$ records and their associated lake basin parameters (Kaufman et al., 2020) or instead they have a limited temporal focus (Konecky et al., 2020). Consequently, no study has yet empirically linked the signal properties of $\delta^{18}O_{BSi}$ records and lake basin parameters in a harmonized dataset.

To overcome these gaps, this paper aims at providing a comprehensive compilation and combined statistical evaluation of all lake sediment $\delta^{18}O_{BSi}$ records published to date (between 1998 and 2022). We accomplish these objectives by means of the following working steps: (1) collecting available lake sediment $\delta^{18}O_{BSi}$ records published to date, (2) complementing these records with the individual lake basin parameters, (3) assessing the signal properties of $\delta^{18}O_{BSi}$ records with regard to lake basin parameters, and (4) identifying spatio-temporal patterns and trends in the $\delta^{18}O_{BSi}$ signals. This effort leads to a better understanding of the general constraints for interpreting lake sediment $\delta^{18}O_{BSi}$ records, whilst making these records more readily usable for future studies including proxy-model comparisons. It is hence a contribution to bridge the gap between modelling and isotope geochemistry approaches in paleoclimate science.

2 Methods

This study follows a three-stage approach: the first stage (data acquisition) comprises identifying lacustrine $\delta^{18}O_{BSi}$ datasets and publications published to date. A second stage includes acquiring the actual $\delta^{18}O_{BSi}$ datasets and archiving them in a standardized format. Where appropriate, the identified published datasets were arranged into longer continuous records. This includes records from the same sediment core published in different papers and records from different sediment cores from the same lake but similar locations. The third and final stage (record analysis) interprets the lacustrine $\delta^{18}O_{BSi}$ isotope records with respect to their hydrological and geographical constraints in order to identify possible common global or hemispheric trends and signal properties of all isotope records, as well as smaller spatially or temporally constrained datasets.

Identification and acquisition of the datasets and publications in this work followed an additive approach, i.e. thorough literature survey. We have chosen this approach due to the limited number of laboratories and working groups worldwide measuring $\delta^{18}O_{BSi}$. In this study, we focused exclusively on down-core records from lacustrine sediments. Identified publications and datasets were entered into a uniform metadata table giving one entry to each publication and each dataset. If more than one publication was written about the same sediment core, each of these publications were given a separate entry. Likewise, if one publication presents data from more than one sediment core, each of the sediment cores were given a separate entry to the database.

For each of these entries, metadata on coring procedure, hydrological setting, and chronology were supplemented. Data were extracted from the corresponding publication(s), from public repositories, or directly from the authors. Hydrological parameters such as catchment area, average depth,

and t_{res} were additionally obtained from the HydroLAKES database (Messager et al., 2016) and stored as separate variables. For a detailed description on how the values in the HydroLAKES database were created, we refer to Messager et al. (2016). This procedure was necessary because original publications do not always specify all of these parameters and because parameters supplied in original publications may not be consistent. For further analysis and for linking the individual isotope records with lake basin parameters, the HydroLAKES database entries were given preference. Original publications were only used for lakes where no data were available from the HydroLAKES database. The parameter "maximum water depth" was always taken from the original publications since this parameter is not provided by the HydroLAKES database. While the geo-statistical approach of the HydroLAKES database may not provide the most precise values for individual lake basin characteristics, it ensures comparability among the different lake basins analysed in this study. Therefore, and because some parameters (i.e. catchment size) are not essential to the discussion in this paper, we have chosen this approach favouring consistency over more data points. It also prevents potential issues arising from different authors providing conflicting values for the same lake basin (i.e. Lake Baikal, Lake El'gygytgyn).

Isotope datasets for each of the entries were archived in separate tables that specify depth, age, and measured isotope values. Datasets were taken directly from the respective publication, where possible. If datasets were not available, within the original publications or their supplements, public repositories (e.g. http://www.pangaea.de, last access: August 2022; http://ncei.noaa.gov, last access: August 2022) were searched. In instances where datasets were unavailable from repositories, the lead authors were contacted directly. In case of published data unavailable from repositories or authors, plots of the original publications were digitized if possible (Rietti-Shati et al., 1998; Hu and Shemesh, 2003). Where digitizing plots was not feasible, records were excluded from further consideration; this was the case for Chondrogianni et al. (2004) and Hu et al. (2003).

Chronologies were adapted from the original publications, where available, and stored in cal yr BP format (relative to 1950 CE). Sample ages given in different formats (e.g. b2K or CE) were converted to cal yr BP. This procedure also applies to radiocarbon-based chronologies. Chronologies were not recalculated because the effect of different ^{14}C calibrations and different age model approaches is presumably minor with regard to the aim of this study. This is especially true when considering the fact that high-resolution datasets (annual to decadal resolution) are the exception among all datasets identified. The error introduced by the different age models is thus considered minor when compared to the resolution of the datasets. For applications requiring more precise chronologies and better comparability of datasets, we provide the radiocarbon measurements of respective datasets as well. This enables future users to create tailor-made chronologies if needed. Datasets without chronologies were stored using depth notation only.

For further analysis, datasets were partly regrouped and combined to generate longer continuous $\delta^{18}O_{BSi}$ datasets, herein referred to as "records". This comprised treating datasets with data from several coring sites or outcrops from the same lake as one single record, in agreement with the author's original interpretation (Quesada et al., 2015; Swann et al., 2018). Data stemming from the same sediment core but published in different papers were combined into single continuous records. This applies to records from Lake Kotokel (Kostrova et al., 2013a, b, 2014, 2016) and Lago Chungará (Hernandez et al., 2008, 2010, 2011, 2013). Likewise, data from different cores presented in different publications but stemming from identical or reasonably similar coring sites were combined to single records. This applies to data from Lake Nar (Dean et al., 2018) and Vuolep Allakasjaure (Rosqvist et al., 2004; Jonsson et al., 2010). Lakes consisting of several basins were generally treated as one, such as Lake Baikal and several smaller lakes.

For trend analysis and inter-comparison, we focused primarily on the Holocene and Common Era climate using records from Northern Hemisphere (NH) extratropical lakes (45–90° N) due to there being the highest spatial–temporal coverage of data with a significant number of records, which makes an interpretation departing from case studies feasible.

In a first step, records were binned to 1 kyr intervals (for the Holocene) and 200 year intervals (for the CE), respectively. These intervals were chosen based on the temporal resolutions of the original records in order to ensure continuous binned records with no empty bins. Choosing higher resolutions would have resulted in many records having empty bins with no data points, thus leading to different temporal resolutions even after binning. The binning was done by calculating the mean value of all samples within the respective age interval for each individual record. Data points with ages < 150 yr BP were excluded from the Holocene analyses to eliminate any possible effects of recent warming, though these data were retained for analysing the Common Era. To assess the timing of Holocene maxima and minima, records covering fewer than 10 bins were discarded. To evaluate Holocene and Common Era trends in $\delta^{18}O_{BSi}$, records covering less than seven bins were excluded from the analysis (i.e. < 7.0 and 1.4 kyr, respectively). Obviously, the missing bins in both Holocene and Common Era compilations might have an effect on the mean value of the individual records but not on the overall trend.

In order to eliminate offsets between individual binned records, the remaining records were standardized by subtracting their respective means. After this mean removal, two subsequent filtering steps were performed in order to exclude records most prone to secondary lake evaporation. First, a subset consisting only of records from open lakes was created, discarding records from semi-closed lakes, closed lakes, and paleo-lakes. In a second step, this open-lakes sub-

set was filtered by discarding all records with $t_{res} > 100$ years. This threshold was chosen in accordance with previous works classifying lakes and their isotopic signals with respect to hydrologic setting and t_{res} (Leng and Marshall, 2004).

After applying these filters, combined trends for geographical regions (NH, Eurasia, North America) were evaluated by calculating the mean of all records for each bin, in each respective region.

3 Results

3.1 Published datasets

Following a thorough literature survey, a total number of 71 published down-core datasets of $\delta^{18}O_{BSi}$ from 64 sites have been identified. Since the first published lacustrine $\delta^{18}O_{BSi}$ studies in 1998 (Rietti-Shati et al., 1998; Shemesh and Peteet, 1998), there has been a growing research interest and number of publications (Fig. A1). Only recently has there been a stagnation of the number of records published. A detailed overview of the identified publications and the records presented therein is provided in Table A1.

Most publications present the $\delta^{18}O_{BSi}$ data as time series, as is usual in paleoenvironmental studies. The chronologies rely on a wide variety of dating methods (Fig. A2), with ^{14}C (used on 46 records) being by far the most frequent. For sub-recent time periods and shorter timescales, ^{210}Pb and ^{137}Cs are also used extensively (on 21 and 12 records, respectively). Globally or regionally correlated time markers such as tephra layers (Heyng et al., 2015) or high-resolution methods such as varve counts (Rozanski et al., 2010) are used relatively sparsely as they are not available for all time periods and/or lake basins.

3.2 Combined records

We combined separate records from the same lake sites to longer, continuous composite records, giving a total of 53 combined $\delta^{18}O_{BSi}$ records. Six of these are from paleolakes (three with or without chronology), while 47 records stem from extant lakes (42 with and five without chronology). An overview of these combined records is provided in Table A2, complemented by metadata of the records and the corresponding lake basins. Each individual record received a number (#X; Table A2, column 1; Table A1, last column) which is used consistently throughout the text.

The temporal coverage of these combined records (Fig. 2) varies from centennial-scale at Laguna Zacapu (#50, Leng et al., 2005) and a specific study at Lake Baikal (#51, Swann et al., 2018), to glacial–interglacial cycles, e.g. 250 kyr at Lake El'gygytgyn (#3, Chapligin et al., 2012b). Most records ($N = 32$) cover the last several thousand years up to about 10 kyr BP, while only a few records cover several tens of thousands of years (e.g. #8 to #10). Likewise, the time periods covered do vary either due to the availability of lake sediments, diatom abundances in a lake and/or scientific foci of the research groups. By far the highest number of records is available for the Holocene (0–11.7 kyr BP; $N = 37$) and especially for the last 2 kyr BP ($N = 48$). Further back in time, Marine Isotope Stages (MISs) were used for assessing data coverage throughout time. Boundaries between MISs are according to Lisiecki and Raymo (2005). MIS 2 is still covered by 19 records, whereas towards MIS 3 ($N = 5$) and beyond fewer records have been generated. However, single records cover even older time periods in MIS 11 (at Lake Baikal; #2) and beyond (MIS G1/104, #1), outlining the applicability of this proxy across a wide range of timescales. A paleolake from the Baringo–Bogoria basin (#1) is the oldest lacustrine $\delta^{18}O_{BSi}$ record and has been dated to the onset of MIS 104 in the late Pliocene (Wilson et al., 2014b).

Regarding the number of published records by continent (Fig. 3), there is a clear concentration on Asia and Europe with 21 and 15 records published, respectively. In Asia, there is a strong regional focus on Siberia, whereas most other parts of the continent are yet to be investigated using lake sediment $\delta^{18}O_{BSi}$. A regional focus also occurs in Africa and South America. While a sizeable number of records stemming from these continents have been published ($N = 10$ and $N = 11$, respectively), there are pronounced regional foci in the East African Rift and the Andes, respectively. Another focus region is Alaska, where most ($N = 6$) of the published North American records ($N = 7$) are located. $\delta^{18}O_{BSi}$ work has also been carried out in lakes from New Zealand (#42) and South Georgia (#19).

In summary, the distribution of available $\delta^{18}O_{BSi}$ data displays a bias towards the mid- to high latitudes of the Northern Hemisphere. Additionally, this distribution is also indicative of the site accessibility and (regional) research foci of the working groups. This has a rather pronounced effect on the spatial distribution of available $\delta^{18}O_{BSi}$ records. The geographical distribution is also indicative of cold regions devoid of carbonates where biogenic silica is the most promising archive to obtain oxygen isotope records from lake sediments. Moreover, high northern latitudes have by far the highest abundance of total area of waterbodies (Downing and Duarte, 2009). Yet, it also accounts for the relatively lower number of northern records extending beyond MIS 1, as vast ice sheets covered much of the NH high latitudes (e.g. Patton et al., 2016).

This pattern also affects the latitudinal distribution of the records (see also Table A2) with records ranging from 54.17° S (#19) to 69° N (#39). Records stemming from low-latitude lakes (particularly in Africa and South America) are often located at high altitudes above 3000 m a.s.l. (above sea level; e.g. #11, 17, 18, 21). Lake Simba Tarn (record #34) features the maximum altitude for an individual $\delta^{18}O_{BSi}$ record of 4959 m a.s.l.. Altitudes below 1000 m a.s.l., however, are most common ($N = 36$), especially for high-latitude lakes. In total, 12 lakes are located below 100 m a.s.l. (e.g. #29, 35). Many of these low-altitude lakes are located in mar-

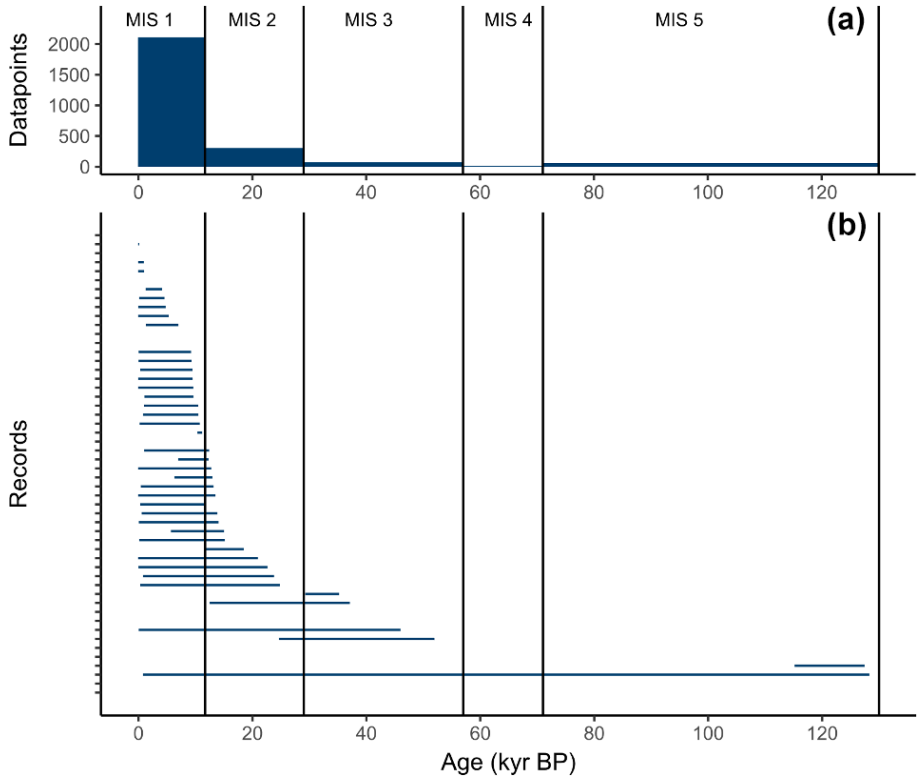

Figure 2. Temporal coverage by records and data points during MIS 1–MIS 5. Boundaries between MIS according to Lisiecki and Raymo (2005): MIS 1–2: 14 kyr; MIS 2–3: 29 kyr; MIS 3–4: 57 kyr; MIS 4–5: 71 kyr; MIS 5–6: 130 kyr. **(a)** Total number of data points available during each Marine Isotope Stage. **(b)** Temporal coverage of records from young to old.

itime locations in immediate proximity to the coast (e.g. #19, 30) or have even had marine intrusion stages in the past (a postglacial transgression at Nettilling Lake; #41). Extremely continental environments are tackled in central and eastern Siberia and the Lake Baikal region (e.g. #4, 8, 9, 10, 25).

3.3 Spatial coverage and resolution of combined records

Varying spatial resolution among the compiled isotope records is linked to the fact that lakes and their corresponding catchments are not points in space but areas. Consequently, lake water and the related $\delta^{18}O_{BSi}$ signal represent a spatial average integrated over the catchment size of each respective lake. Lake surface areas range from small ponds of $< 1\,km^2$ (e.g. #19, 11, 23, 33, 34) to some of the largest lakes in the world, including Lake Malawi and Lake Baikal covering 29 544 and 31 968 km^2 , respectively (Fig. 4a). Large and voluminous lakes are the exception, however, and most of the lakes represented here are $< 10\,km^2$ in size ($N = 25$). Note that such parameters are not applicable to paleolakes. While some authors provide estimates on paleolake extent, these figures are not consistent with the values determined for present lakes and are therefore not included in the evaluation of the dataset. Catchment sizes vary by several orders of magnitude as well. For small lakes, catchments are often $< 10\,km^2$ ($N = 13$; e.g. #22, 33, 37), whereas the largest lakes, Lake Malawi and Lake Baikal, feature catchments of 128 727 and 569 176 km^2, respectively (Fig. 4a). Therefore, these lakes integrate the environmental signal over a large and potentially diverse hydrological region. While most of the lakes compiled in this study are primarily fed by surface runoff and/or precipitation (according to the original publications of records), groundwater influx may also play a pivotal role by introducing a large memory effect of past precipitation due to the generally long residence times of aquifers. This may have an impact on records especially when looking at short timescales. Groundwater input, however, is usually not accounted for and is thus beyond the scope of our study. In summary, both lake and catchment sizes vary by several orders of magnitude (Fig. 4a) among the sites with existing $\delta^{18}O_{BSi}$ records and span from local signals to regional averages. However, most of the records ($N = 18$) stem from lakes with catchments $< 100\,km^2$, suggesting rather local signals. While single local signals represent small areas, different local signals may well correlate on continental and hemispheric scales.

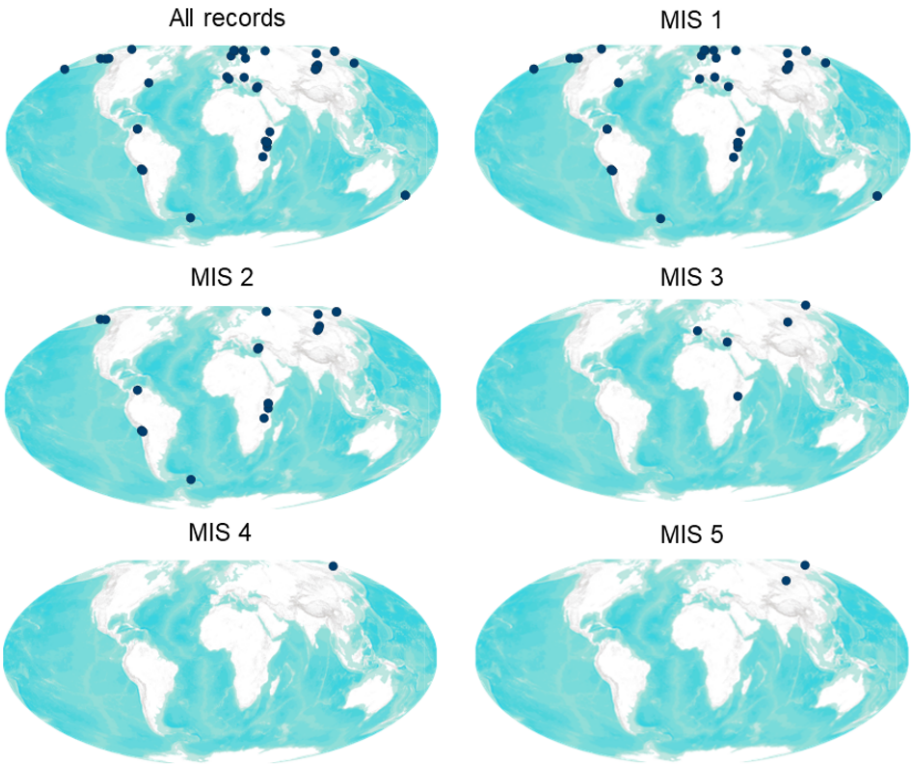

Figure 3. World map depicting the locations of $\delta^{18}O_{BSi}$ records with chronology. Note that one location may correspond to more than one record. © Esri 2022.

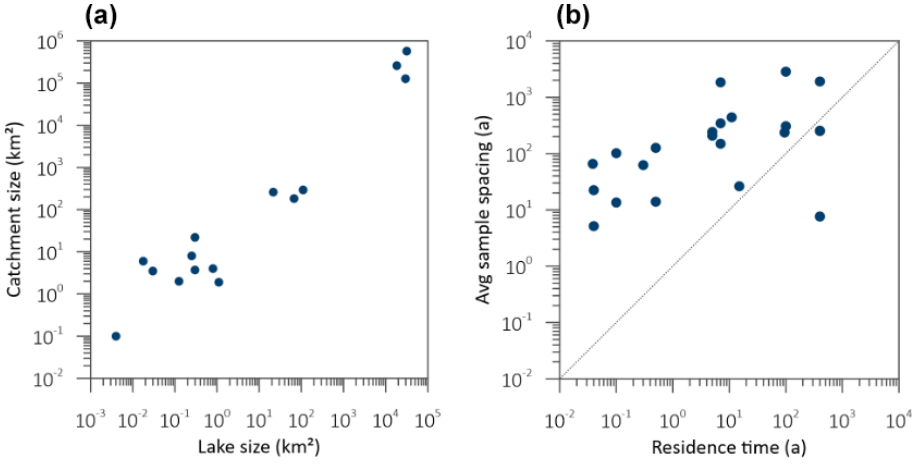

Figure 4. **(a)** Depiction of corresponding lake and catchment sizes of the records compiled within this study. One lake may correspond to more than one record. Note that records from paleo-lakes and lakes with incomplete information on lake and catchment size were not considered for this figure ($N = 33$). **(b)** Depiction of corresponding sampling intervals and t_{res}. Note that records from lakes without information on t_{res} were not considered for this figure ($N = 37$).

3.4 Temporal resolution of combined records

Temporal resolution of the records and the resulting signal properties are determined by both the lake basin itself (i.e. accumulation rates and preservation of diatom silica) and the sampling routine applied to the sediment core (i.e. the sampled intervals as well as the thickness of individual samples). Data on the thickness of single sediment samples taken from the cores are, however, scarce in the original publications. The same applies for information on the time interval or number of years represented by a single sediment sample. Consequently this parameter and its potential effect on the records' signal properties could not be investigated in detail

in this paper. We therefore focus on t_{res} and sampling frequency of a core as a means of characterizing the records and their temporal resolution.

The t_{res} is closely linked to the size of lake basins and varies accordingly. It ranges from several weeks for small lakes (e.g. #49, 50) to centuries (219 and 375 years for Lake Malawi and Lake Baikal, respectively). On the whole, t_{res} of sub-annual to annual scale are most common ($N = 17$) among the lakes considered in this study (Fig. 4b). It should be noted that longer t_{res} leads to averaging of the signal over a longer time period. Likewise, different t_{res} may also have an effect on absolute $\delta^{18}O_{BSi}$ values and variabilities. Lakes with very long t_{res} ($t_{res} > 100$ years) are more susceptible to lake evaporation, and may effectively behave like closed-system lakes with regard to the $\delta^{18}O_{BSi}$ signal even if they are hydrologically open (i.e. have outflows). These are still referred to as hydrologically open in this work and hydrological settings and t_{res} are addressed separately in the discussion.

The sampling frequency also varies by several orders of magnitude (Fig. 4b). It stretches from annual to multi-millennial timescales. Consequently, the signal properties and the recorded climatic and/or hydrological forcings of the identified records can be expected to vary accordingly. Most records, however, plot in the top left half of graph of Fig. 4b, which indicates that the temporal offset between two sediment samples exceeds t_{res}. This suggests that the sampling routine is the limiting factor of the temporal resolution of these records. Only three records from Lake Baikal plot in the lower-right half of Fig. 4b, suggesting t_{res} to be the dominant factor in determining the record's resolution in these cases (#4, #20, #51), at least with respect to inflow-related changes.

We thus conclude that the sampling resolution is the main factor determining the temporal resolution of most records, with t_{res} acting as an additional smoothing mechanism. A lake with a centennial-scale t_{res} can, therefore, display centennial-scale changes in climate and hydrology to their full amplitude. Decadal-scale changes, on the other hand, can be expected to be attenuated by an order of magnitude in a lake with centennial-scale t_{res}. When t_{res} is lower than the sampling frequency, the hydroclimatic amplitude is also not fully captured (Richter and Turekian, 1993). It should be noted that temporal resolution is non-uniform across the records, with generally higher resolution for more recent time intervals (Figs. 2 and 5a) that – in addition to a sampling bias – may in part reflect increasing lake sediment compaction with depth and time. Based on t_{res} and sampling resolutions of the records, comparing records on a centennial or millennial scale is the most promising approach for assessing common patterns.

4 Discussion

4.1 Common Era climate

For analysis of Common Era climate, only data points from 0 CE until today (corresponding to 1950 to −73 yr BP) were selected. The Common Era subset of records includes only records stemming from sites north of 45° N (Fig. 5a, $N = 19$) and comprises 460 data points. The records display considerable offsets with $\delta^{18}O_{BSi}$ values ranging from +19 ‰ (#34) to +33 ‰ (#35) VSMOW. These offsets can be linked to their individual environmental setting, e.g. latitudinal and continentality effects, as well as to their potential to be prone for lake evaporation. Amplitudes in $\delta^{18}O_{BSi}$ of CE records vary from 0.4 ‰ (#24) to ca. 9 ‰ VSMOW (#35). This variability might correspond to their different hydrological settings. Closed lakes (such as Sunken Island Lake; #26) have a tendency towards higher $\delta^{18}O_{BSi}$ amplitude due to evaporative enrichment of the lake water (Broadman et al., 2020b).

Binned records (Fig. 5b, $N = 14$) do not display any common pattern and feature $\delta^{18}O_{BSi}$ values ranging from +20 ‰ to +31 ‰ VSMOW. However, binning of data points and exclusion of shorter records reduces the $\delta^{18}O_{BSi}$ amplitudes of individual records to less than 5 ‰. Offsets between individual records may be linked to site-specific characteristics of individual lakes and catchments, as well as latitudinal and continentality effects.

After mean removal (i.e. standardization; Fig. 5c), the CE data suggest a common trend with higher $\delta^{18}O_{BSi}$ values at 1900 yr BP and a general decrease until the present, with the lowest values occurring in the last 400 years (two bins). Some records also show maxima between 500 and 1100 yr BP and minima at ca. 1300 yr BP. The subsets for hydrologically open lakes ($N = 13$, Fig. 5d) and hydrologically open lakes with $t_{res} < 100$ yr ($N = 9$, Fig. 5e) show a similar pattern.

The combined CE records (Fig. 5f) comprise eight records and show a general $\delta^{18}O_{BSi}$ decrease over the last 2 kyr amounting to ca. 2 ‰ VSMOW (slope: ~ 1 ‰ kyr^{-1}). The $\delta^{18}O_{BSi}$ amplitude within individual bins, however, might exceed this number, most notably at 100, 1300, and 1900 yr BP, which show the highest amplitudes of up to 5 ‰ for the CE. This is in line with differences between the timing of $\delta^{18}O_{BSi}$ maxima and minima between North American and Eurasian records. At centennial scale, these differences might also be linked to dating uncertainties. Moreover, the record of Lake Bolshoye Shchuchye (#16) features a much larger amplitude. Its exceptional $\delta^{18}O_{BSi}$ variability has been attributed to variations in snow and snowmelt in the lake's catchment and therefore does represents a different kind of precipitation-based signal compared to most other records. The combined trend features its highest $\delta^{18}O_{BSi}$ values at 1900 yr BP, followed by a decrease leading to a relative minimum at 1100 and 1300 yr BP. This phase is followed by a second $\delta^{18}O_{BSi}$ peak at 700 and 900 yr BP, after which a de-

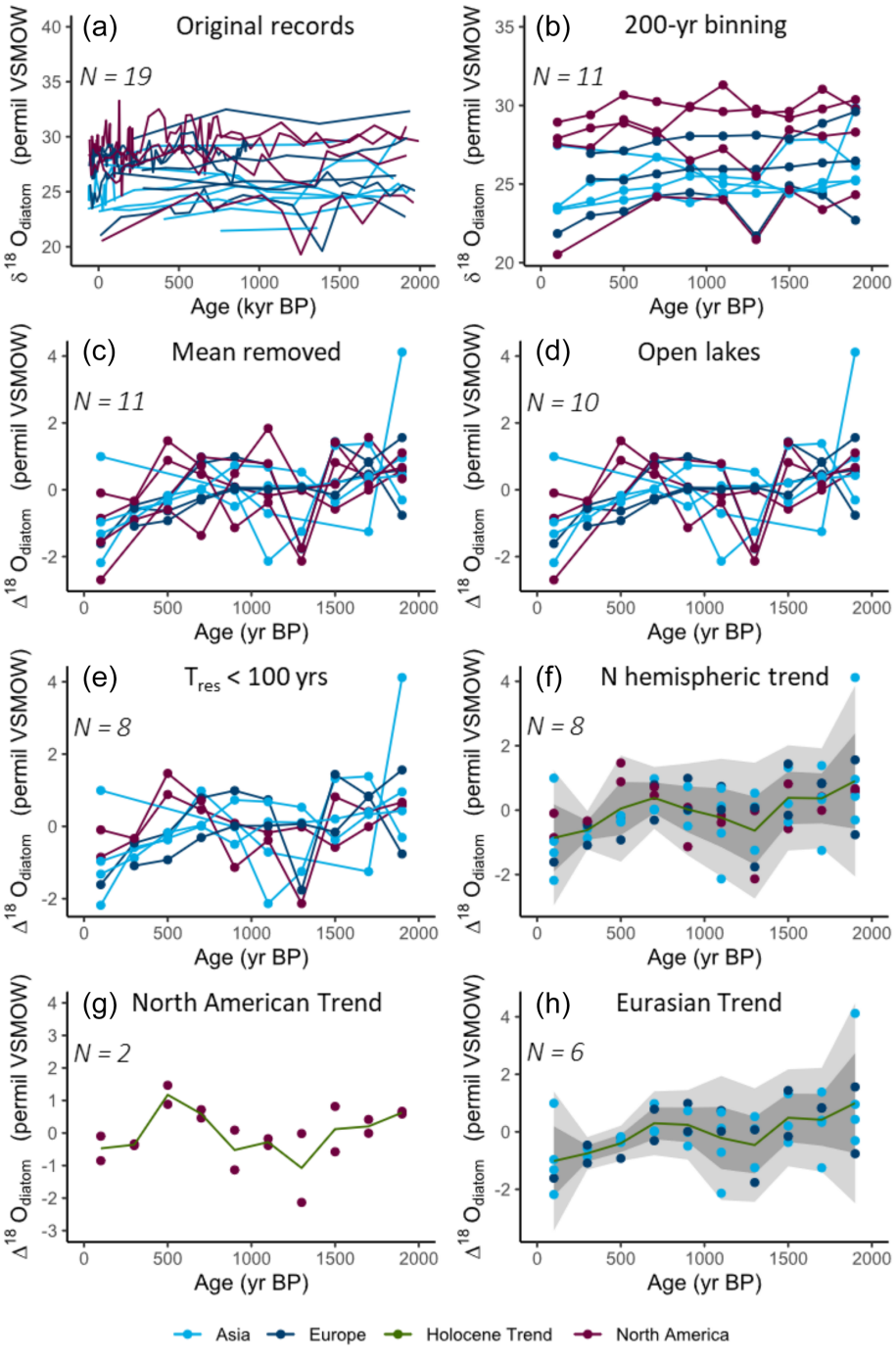

Figure 5. Common Era Northern Hemispheric records (45–90° N) compiled in this study. **(a)** Original records, **(b)** data binned to 200-year intervals only showing records covering at least seven bins, **(c)** binned records with mean of individual records removed, **(d)** data filtered for records from open lakes only, **(e)** data filtered for records from lakes with $t_{res} < 100$ yr, and **(f)** the NH trend calculated as mean of all records in each bin. Shadings show 1 and 2 standard deviations, respectively. **(g)** North American and **(h)** Eurasian trend.

crease can be observed. The decrease at 300 and 500 yr BP features the least deviation between individual records. The most recent bin again shows a much larger $\delta^{18}O_{BSi}$ variability. While most records display the lowest values at this time, Lake Kotokel (#8) for instance shows an increase compared to the previous bins. This increase may or may not be related to recent warming, and due to the complex hydrology of the lake even lake evaporation cannot be ruled out. Most of the records, however, do not indicate a recent $\delta^{18}O_{BSi}$ maximum that might be indicative of recent warming.

It should be noted that there is bias of data points towards the older end of the most recent bin. An absence of recent warming in the data therefore might be linked to this bias, and hence a reaction of lake systems to recent warming cannot be ruled out. As Eurasian records constitute the majority of records ($N = 7$), it is similar to the NH trend (Fig. 5h).

The trends calculated for the last 2 kyr (2K) for the NH (Eurasian) $\delta^{18}O_{BSi}$ stacks are high with $-0.64\,‰\,kyr^{-1}$ ($-0.85\,‰\,kyr^{-1}$) for 10 bins, with even higher slopes of $-1.6\,‰\,kyr^{-1}$ ($-1.7\,‰\,kyr^{-1}$) for bins 6–10 (1 to 2 kyr) and $-1.4\,‰\,kyr^{-1}$ ($-1.8\,‰\,kyr^{-1}$) for bins 1–5 (corresponding to the last millennium). The negative slope is interrupted by three consecutive bins (4–6; 0.6–1.2 kyr BP) plus bin 8 (1.4–1.6 kyr BP) with higher $\delta^{18}O_{BSi}$ than the previous bin. For the last 2 kyr BP, the other five bins (1–3, 7, and 9) show a negative sign for the NH and Eurasian $\delta^{18}O_{BSi}$ 2K reconstructions.

North American records ($N = 2$) do not show a consistently decreasing trend (Fig. 5g) but show slightly higher values at 1.7 and 1.9 kyr BP compared to the most recent bins (0.1 and 0.3 kyr BP, respectively). They do, however, show lower $\delta^{18}O_{BSi}$ values between 0.9 and 1.3 kyr BP, followed by a $\delta^{18}O_{BSi}$ maximum at 500 yr BP. As there are only two records available after filtering, caution has to be applied in interpreting this pattern.

For the North American $\delta^{18}O_{BSi}$ 2K reconstruction, a lower overall gradient is observed ($-0.12\,‰\,kyr^{-1}$), which shows also a steep slope for bins 6–10 with $-1.5\,‰\,kyr^{-1}$. In contrast to the NH and Eurasian $\delta^{18}O_{BSi}$ stack, bins 1–5 show a slight decrease of $-0.4\,‰\,kyr^{-1}$ only. This leads to slightly shifted minima and maxima between $\delta^{18}O_{BSi}$ reconstructions for the last 2 millennia: NH and Eurasian reconstructions have their absolute maxima in bin 10 or at 1.8–2.0 kyr (absolute minima: bin 1; 0–0.2 kyr) with intermediate minima at 1.2–1.4 kyr BP (bin 7) and maxima between 0.6–1.0 kyr BP (bins 4 and 5). In contrast, for the North American reconstruction, the absolute $\delta^{18}O_{BSi}$ minimum (maximum) is at 1.2–1.4 kyr BP or bin 7 (0.4–0.8 kyr BP (bins 3 and 4), whereas the early maximum (bin 10) and late minimum (bin 1) are less pronounced. In summary, we observe an overall decreasing trend in $\delta^{18}O_{BSi}$ for the last 2 millennia for the NH, Eurasian, and North American stacks, which is accelerated in the first millennium.

Similar patterns among Eurasian and possibly NH $\delta^{18}O_{BSi}$ records do suggest a common NH signal throughout the CE. The observed maxima and minima correspond to previously described climatic events, notably the Roman Warm Period from 2.0 kyr BP to about 1.6 kyr BP (Ljungqvist, 2010), the Dark Ages Cold Period from 1.6 to 1.2 kyr BP (Büntgen et al., 2016; Helama et al., 2017), the Medieval Climatic Anomaly (MCA) from 1.2 to 0.8 kyr BP (Bradley et al., 2003; Mann et al., 2009), and the Little Ice Age from 0.7 to 0.1 kyr BP (Matthews and Briffa, 2005; Wanner et al., 2022). In Fig. 5f, the two main cold phases (Dark Ages Cold Period and Little Ice Age) are clearly represented. The good accordance of our data with these previously described warm and cold phases suggests that $\delta^{18}O_{BSi}$ records presented are influenced by T_{air} change, either directly or via other parameters linked to T_{air}. Recent research has rejected the global nature of these climatic events and suggested that they are regionally constrained (Neukom et al., 2019). However, the accordance of our data – when assessed at centennial scale – with these climatic events is expected because they were initially described for North America and Europe.

4.2 Holocene (corresponding to MIS 1) climate

To facilitate comparison with other Holocene reconstructions, for deriving Holocene trends only 12 kyr (in 1 kyr bins) are considered, and the boundary between MIS 1 and MIS 2 is set to 12 kyr. Thus, the Holocene NH subset of records (covering the past ca. 12 kyr) consists of 21 records that display a considerable range in mean $\delta^{18}O_{BSi}$ values from +20 ‰ (#3) to +35 ‰ (#31) VSMOW (Fig. 6a) that reflect local site-specific difference. For example, Lake El'gygytgyn (#3) is located in a continental, high-latitude environment with little secondary evaporation (Chapligin et al., 2012b), whereas Lake Ladoga (#31) is situated in a less continental, lower-latitude setting with a complex hydrological history of changing inflows and outflows (Kostrova et al., 2019).

Amplitudes of the individual Holocene records vary from less than 5 ‰ (#3) to ca. 10 ‰ VSMOW (#20, #35). Lake El'gygytgyn (#3) is a voluminous, deep hydrologically open lake with little lake evaporation, whereas Heart Lake (#35) is a much smaller, less voluminous lake with a short t_{res} (2 weeks). Lake Baikal (#20) is a deep voluminous lake like Lake El'gygytgyn, but it has a centennial-scale t_{res} making it effectively closed and thus potentially subject to secondary evaporation. Consequently, differences in their isotopic variability might correspond to their different hydrological settings. Closed lakes (such as Sunken Island Lake; #26) have a tendency towards higher $\delta^{18}O_{BSi}$ values that are likely due lake evaporation leading to a more enriched isotope signature of lake water (Broadman et al., 2020b; Hernandez et al. 2008).

Binned records (Fig. 6b, $N = 14$) do not display any common patterns and feature $\delta^{18}O_{BSi}$ values ranging from +20 ‰ to +35 ‰ VSMOW, similar to the original records. However, binning of data points and exclusion of shorter records results in smoothed amplitudes of less than 5 ‰ VSMOW. The binned records exhibit Early Holocene $\delta^{18}O_{BSi}$ values (up to 2.5 ‰) higher than the Holocene mean, whereas late Holocene values are generally up to 2 ‰ below the Holocene mean. However, some records do not follow this general pattern after mean removal (Fig. 6c). This could be indicative of the different hydrological settings and t_{res} which have a substantial impact on the recorded signal.

Filtering for hydrologically open lakes (Fig. 6d, $N = 13$) and $t_{res} < 100$ yr (Fig. 6e, $N = 10$) displays a clear decreasing $\delta^{18}O_{BSi}$ trend of 2.5 ‰ throughout the Holocene. However,

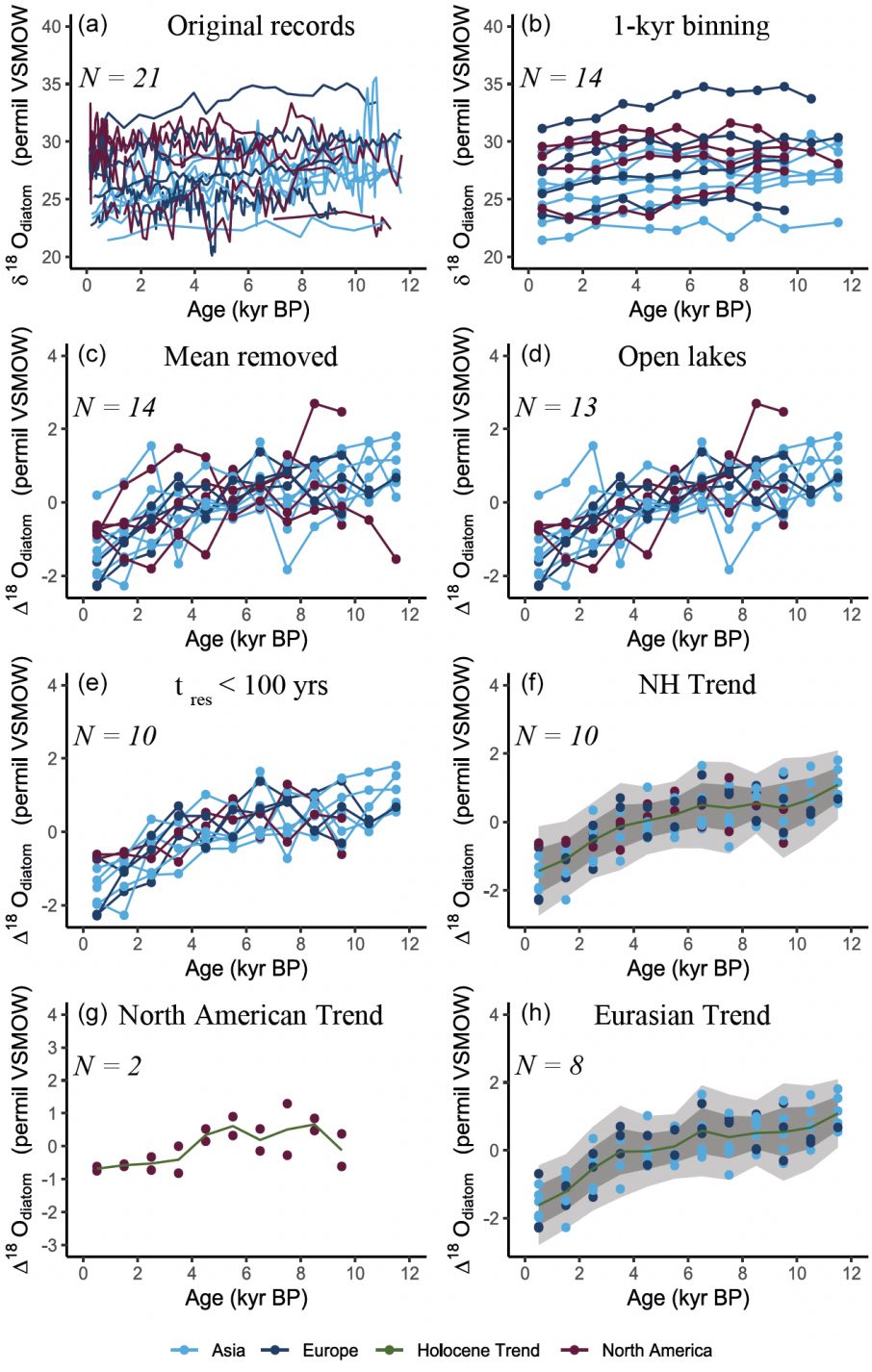

Figure 6. Holocene Northern Hemispheric records (45–90° N) compiled in this study. **(a)** Original records, **(b)** data binned to 1 kyr intervals only showing records covering at least 7 bins, **(c)** binned records with mean of individual records removed, **(d)** data filtered for records from open lakes only, **(e)** data filtered for records from lakes with $t_{res} < 100$ yr, and **(f)** the NH trend calculated as mean of all records in each bin. Shadings show 1 and 2 standard deviations, respectively. **(g)** North American and **(h)** Eurasian trend.

differences between individual records do exist, and most notably the absolute $\delta^{18}O_{BSi}$ maxima of individual records do not occur at the same time. While some records feature maxima at the beginning of the Holocene, other records peak between 5 and 8 kyr BP. This pattern is in line with Holocene T_{air} reconstructions which have found spatial differences of the timing of the Holocene thermal maximum (Kaufman et al., 2004; Renssen et al., 2009).

Based on this subset of hydrologically open lakes with $t_{res} < 100$ yr, a combined millennial-scale NH trend was calculated. This combined Holocene trend (Fig. 6f) shows a decrease throughout the Holocene amounting to ca. 2 ‰ VSMOW. The absolute maximum is observed for the Early Holocene bin at 11–12 kyr BP. A decrease at the beginning of the Holocene between 12 and 10 kyr BP is followed by a relatively stable middle Holocene until 6 kyr BP and subsequent stronger decrease towards the absolute $\delta^{18}O_{BSi}$ minimum in the youngest bin (0–1 kyr BP).

When considered separately, North American ($N = 2$) and Eurasian ($N = 8$) records show different patterns and have been described and interpreted differently in the case studies published to date. While the former are primarily linked to atmospheric circulation changes in Alaska (Bailey et al., 2018; Broadman et al., 2020b, a), the latter are at least partly interpreted as indicative of T_{air} and insolation changes (Swann et al., 2010; Mackay et al., 2011; Chapligin et al., 2012b; Kostrova et al., 2013a, 2019, 2021). Eurasian $\delta^{18}O_{BSi}$ records ($N = 8$) display a slight decrease from 12 kyr BP to 10 kyr BP and suggest a second maximum at 7 kyr BP followed by a second relatively stable phase. An accelerated decrease starting at ca. 4 kyr BP constitutes a more abrupt change than in the NH trend. The Holocene trend calculated for the NH (Eurasian) $\delta^{18}O_{BSi}$ stack is -0.19 ‰ kyr^{-1} (-0.21 ‰ kyr^{-1}) for all 12 bins, with a lower slope of -0.11 ‰ kyr^{-1} (-0.10 ‰ kyr^{-1}) between 12–7 kyr BP and a much higher slope of -0.39 ‰ kyr^{-1} (-0.36 ‰ kyr^{-1}) for bins 1–6 (corresponding to 6–0 kyr BP).

Throughout the Holocene, 10 out of 12 bins are lower than the previous one (i.e. negative sign) for the NH $\delta^{18}O_{BSi}$ reconstruction, except between 9–8 and 7–6 kyr BP (bins 9 and 7), which show an increase in $\delta^{18}O_{BSi}$. For the Eurasian $\delta^{18}O_{BSi}$ stack all bins are lower in $\delta^{18}O_{BSi}$ than the preceding one (except for bin 7, or 7–6 kyr BP, which shows an increase of +0.2 ‰). The most negative slopes exceeding -0.55‰ kyr^{-1} are observed between 2–1 kyr BP for both the NH and the Eurasian compilation. For the North American $\delta^{18}O_{BSi}$ reconstruction, a slightly lower trend is observed for the Holocene (-0.13 ‰ kyr^{-1}, based on 10 bins), which also shows a steeper slope between 5–0 kyr BP (bins 5–1) with -0.22 ‰ kyr^{-1}. In contrast to the NH and Eurasian $\delta^{18}O_{BSi}$ stack, there is a slight increase of +0.10 ‰ kyr^{-1} between 10–6 kyr BP (bins 10–6), likely driven by bins 6 and 9, which are the only ones showing a positive sign, whereas all 7 other bins show a decrease compared to the preceding one.

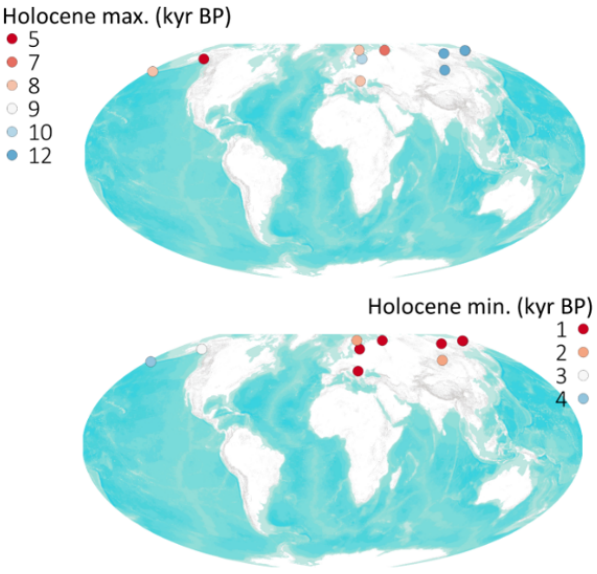

Figure 7. Timing of $\delta^{18}O_{BSi}$ maxima and minima of binned records in the Holocene. Filter criteria are the same as indicated in Fig. 10, and only records covering at least 10 bins have been considered. © Esri 2022.

Hence, North American records do not show a consistently decreasing trend throughout the Holocene (Fig. 6g) but instead slightly higher $\Delta^{18}O_{BSi}$ values in the first half of the Holocene as compared to the second half. Since there are only two North American records fulfilling our selection criteria, it is difficult to meaningfully go beyond the existing case studies, outlining the necessity for further research in this region. In summary, we observe a mostly continuous decrease in $\delta^{18}O_{BSi}$ throughout the Holocene for the NH, Eurasian and North American stacks, which is accelerated in the second half of the Holocene. This phenomenon has been previously described as Neoglacial Cooling (e.g. McKay et al., 2018).

The regional differences between North America and Eurasia are also manifested in the timing of absolute $\delta^{18}O_{BSi}$ minima and maxima of individual records (Fig. 7). The spatial pattern of the Holocene maxima of binned records shows a different timing of maxima for different regions (Fig. 7). Eastern Eurasian sites feature a pronounced early Holocene maximum (at 12 kyr BP), whereas sites to the west of Eurasia show a tendency towards rather a middle Holocene maximum, around 8–6 kyr BP. This suggests that the double maxima of the Eurasian trend (Fig. 6h) is at least partly caused by the regional differences over Eurasia. There are also individual records, however, which do show two peaks within the Holocene, e.g. Lake Bolshoye Shchuchye from the polar Ural Mountains (#16). Records from Alaska feature later $\delta^{18}O_{BSi}$ maxima (5 and 8 kyr BP, respectively).

The timing of Holocene minima is rather consistent across northern Eurasia, where all records reaching their minimum

in the last 1 kyr BP or between 2 and 1 kyr BP (Fig. 7). While the records generally follow the same decreasing long-term $\delta^{18}O_{BSi}$ trend, they feature either early or late Holocene minima. Since data points of 1850 CE and younger have been removed from the dataset prior to analysis to exclude the industrial era, a potential effect of recent climate change is not covered in this subset of data. As with the Holocene maximum, sites in Alaska also differ with regard to the Holocene minimum. They show a tendency towards absolute minima earlier than Eurasian records (between 3 and 4 kyr BP, respectively). Despite the scarcity of the records fulfilling the selection criteria, this suggests a different behaviour of the regions (North America and Eurasia), though we also acknowledge that one of the two North American sites (#35, Heart Lake) is located in the central northern Pacific Ocean and has a different climatic history.

The African ($N = 7$) and South American records ($N = 3$) do not fulfil the criteria set for the NH and Eurasian stacks due to either hydrological or temporal constraints (e.g. too few data points). However, all three South American records (see Table A2; #18, 28, 32) show an early Holocene maximum around 10 kyr BP. Two out of three South American $\delta^{18}O_{BSi}$ records show a decrease over the Holocene, whereas the third record displays no clear trend.

Due to marked differences in hydrology among sites, an African $\delta^{18}O_{BSi}$ stack has not been calculated either. Instead, individual records ($N = 5$) have been compiled and binned separately for the African continent (Fig. A5a and b). We observe the largest $\delta^{18}O_{BSi}$ variability within one individual record ($\delta^{18}O_{BSi}$ range of ca. 20 ‰, #21) as well as highest absolute $\delta^{18}O_{BSi}$ (with values up to +45 ‰, #33). This is related to the very different settings both in altitude (Table A2) and hydrological characteristics (Fig. A5d). Overall, the first half of the Holocene is characterized by slightly lower $\Delta^{18}O_{BSi}$ values than the second half. As this observation is less obvious for open lakes (Fig. A5d), a bias linked to widely different hydrological settings of the respective lakes (see Table A2) has to be assumed, which renders it difficult to disentangle the drivers of $\delta^{18}O_{BSi}$. This further underscores the importance of hydrologically constrained records to infer a common (climate) signal (see Figs. 5a and 6a).

4.3 Combined Holocene trend in the hemispheric context

The combined trends of $\delta^{18}O_{BSi}$ for the NH, Eurasia, and North America are shown in comparison to other NH proxy records in Fig. 8. As individual $\delta^{18}O_{BSi}$ records are commonly discussed with respect to insolation, we also include June and December insolation curves for 60° N (Laskar et al., 2004, Fig. 8f). As shown in Fig. 8g and h, Eurasian and NH combined trends show a similarity with the June insolation as all records feature a decreasing trend throughout the Holocene. However, insolation decreases steadily after an early Holocene maximum, whereas combined NH and Eurasian $\delta^{18}O_{BSi}$ trends feature a stable early Holocene and a second peak at 7 kyr BP. This presumably relates to the geographical distribution of the timing of $\delta^{18}O_{BSi}$ maxima and minima as discussed above. Therefore, eastern Eurasian records are most in line with June insolation, which has been regarded as a proxy of summer T_{air} (#3, 24). Records stemming from sites further west are less directly correlated with June insolation. A striking difference is the accelerated decrease of $\delta^{18}O_{BSi}$ after 4 kyr BP in the NH and Eurasian time series, co-incident with Neoglacial Cooling, which is not mirrored in the insolation curve. The relatively stable insolation during this time suggests that the accelerated decrease visible in $\delta^{18}O_{BSi}$ records must be driven by other factors.

Conversely, December insolation (Fig. 8f) shows an anticorrelation with the $\delta^{18}O_{BSi}$ records. However, as both the absolute values and the changes in December insolation are an order of magnitude lower than those of June insolation, a decisive influence of December insolation on $\delta^{18}O_{BSi}$ records can be ruled out. This is in good agreement with previous works, claiming that the $\delta^{18}O_{BSi}$ proxy yields a summer-dominated signal (Shemesh et al., 2001a; Kostrova et al., 2021), supported by the fact that most biogenic production is in late spring–early summer (particularly relevant for NH high-latitude short-residence-time systems). It has to be noted that the records displayed still stem from different latitudes, and the insolation patterns are not identical at all these sites. A decrease in summer insolation, however, is generally the case for high-latitude regions throughout the Holocene.

Temperature reconstructions by Vinther et al. (2009) using $\delta^{18}O$ data from ice cores at Agassiz ice cap and Greenland (between 65 and 80° N) show a pronounced T_{air} increase of about 5 °C at the beginning of the Holocene until 10 kyr BP, followed by a stable phase until 7 kyr BP (Fig. 8a). While the NH and Eurasian $\delta^{18}O_{BSi}$ trends do not feature this increase during the early Holocene, they do show a relatively stable phase from 10 to 7 kyr BP. After 7 kyr BP, both the NH $\delta^{18}O_{BSi}$ trend and the NH T_{air} reconstruction feature a decrease of ca. 2 °C and 1.5 ‰ VSMOW, respectively. As the present-day global average T_{air}-dependent fractionation in precipitation amounts to 0.695 ‰ (°C)$^{-1}$ (Dansgaard, 1964), a 1.5 ‰ $\delta^{18}O$ decrease would thus correspond to a 2 °C cooling, the same T_{air} change as found by Vinther et al. (2009). This good agreement of $\delta^{18}O_{BSi}$ combined trends (NH and Eurasia) and the T_{air} reconstructions by Vinther et al. (2009) suggests summer T_{air} to have a major impact on $\delta^{18}O_{BSi}$ records on millennial timescales.

Multi-proxy-based temperature reconstructions by Marcott et al. (2013) (regional stack 30 to 90° N, Fig. 8b) also show a temperature increase until 10 kyr BP, followed by a stable phase until ca. 7 kyr BP and a decrease of ca. 2 °C thereafter. This temperature reconstruction includes a much broader geographical focus and different land-based and marine proxies (e.g. pollen, chironomids, ice). Thus, the stable phase from 10 to 7 kyr BP and a maximum around 7 kyr BP are shared features of the $\delta^{18}O_{BSi}$ trends of this work, the ice

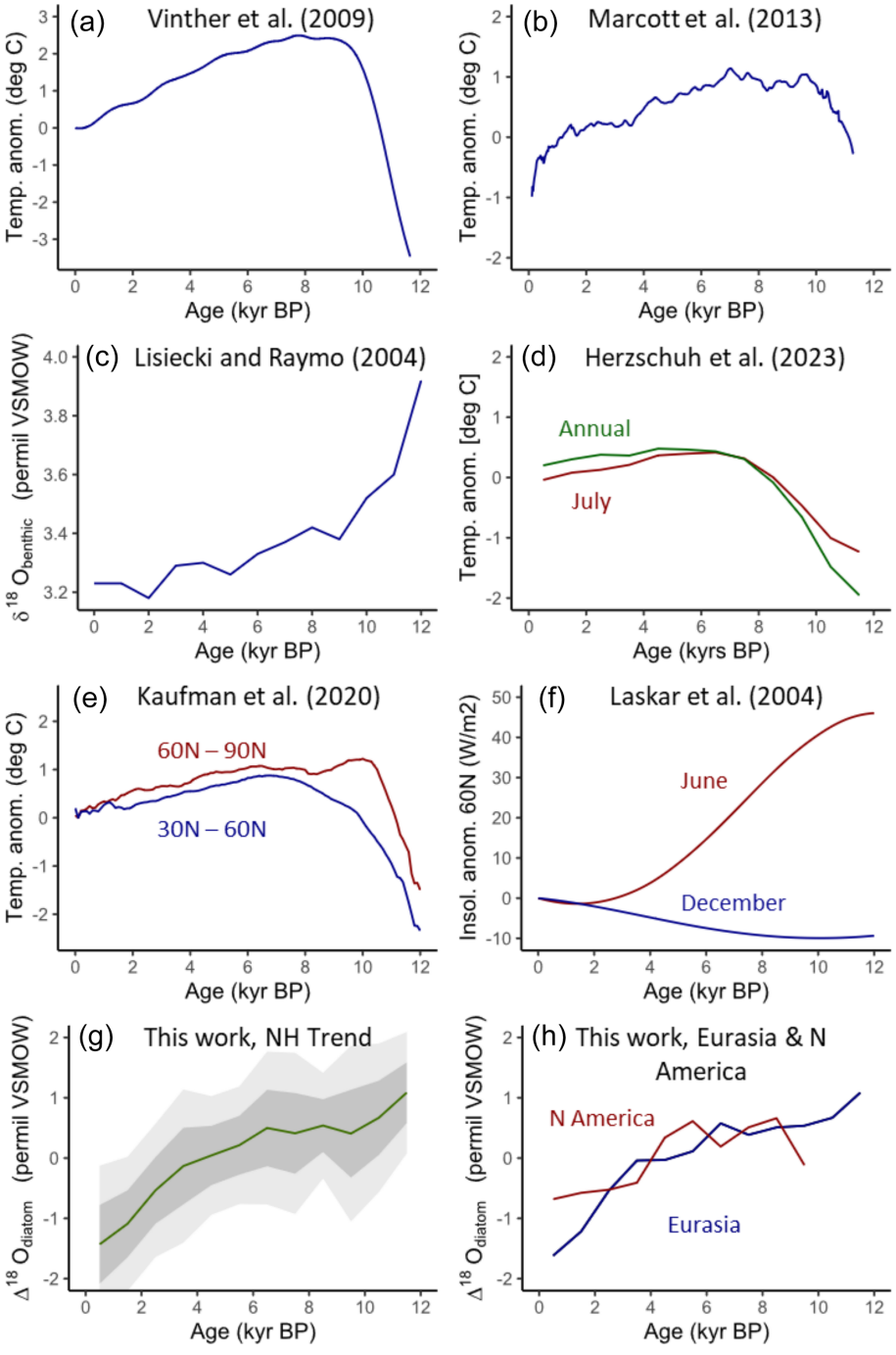

Figure 8. Combined trend of $\delta^{18}O_{BSi}$ compared to other climate reconstructions. **(a)** Greenland ice sheet temperature reconstruction. **(b)** Multi-proxy temperature reconstruction (30–90° N). **(c)** Global stack of $\delta^{18}O$ from benthic foraminifera. **(d)** Temperature reconstruction (45–90° N) based on pollen data. **(e)** Temperature anomalies of mean surface temperatures (multi-method ensemble). **(f)** Insolation anomaly for June and December. **(g)** Combined NH trend from $\delta^{18}O_{BSi}$ records (this work). **(h)** Combined Eurasian and North American trends from $\delta^{18}O_{BSi}$ records (this work).

core reconstruction from Vinther et al. (2009) and the temperature reconstructions by Marcott et al. (2013). However, the early Holocene maximum of the $\delta^{18}O_{BSi}$ trends is not represented in reconstructions by Vinther et al. (2009) and Marcott et al. (2013). This discrepancy might reflect different regional biases of Marcott et al. (2013) and this work, which is also in line with the different timing of Holocene maxima in the $\delta^{18}O_{BSi}$ data (Fig. 8). Given the discrepancy between temperature reconstructions and $\delta^{18}O_{BSi}$ records in the early Holocene, it is likely that the influence of factors other than T_{air} – such as glacial retreat and ice melt during deglaciation – is especially pronounced in the early Holocene. The LR04 stack of the $\delta^{18}O$ of benthic foraminifera (Lisiecki and Raymo, 2005) features continuously decreasing $\delta^{18}O$ throughout the Holocene, which is in accordance with the combined Eurasian $\delta^{18}O_{BSi}$ trend (Fig. 8c).

Pollen records may help to further investigate this issue as they stem from terrestrial environments but are also archived in lake sediments. Moreover, they offer a similar temporal and geographical focus compared to our records, extending to high latitudes. For this comparison we have used the Holocene pollen data compilation by Herzschuh et al. (2021, 2022, 2023a, b) extracting data from 864 records from sites north of 45° N. Changes in annual T_{air} and July T_{air} relative to modern values were retrieved from the pollen dataset. Annual and July T_{air} show similar patterns with a pronounced early Holocene increase, followed by middle Holocene maximum and a less pronounced decrease until the present day (Fig. 8d). Both the middle Holocene maximum and the subsequent decrease in T_{air} are in good agreement with the combined Eurasian $\delta^{18}O_{BSi}$ trend (Fig. 8d and h). This further supports a substantial influence of T_{air} on the $\delta^{18}O_{BSi}$ signal. However, the early Holocene maximum of $\delta^{18}O_{BSi}$ in our combined NH and Eurasian trends is not reflected by pollen-based reconstructions. Caution has to be applied when using pollen-based climate reconstructions for comparison because vegetation changes may lag millennia behind changes in climatic variables (Herzschuh et al., 2016). In summary, the similarity of our combined $\delta^{18}O_{BSi}$ trends with NH temperature reconstructions and insolation data allows for deducing a clear link to summer T_{air} for the Holocene records. Therefore, our $\delta^{18}O_{BSi}$ record contributes to the understanding of the Holocene climate history.

A significant discrepancy between Holocene cooling deduced from proxy reconstructions (e.g. Marcott et al., 2013; Kaufman et al., 2020; Fig. 8b and e) and Holocene warming simulated in climate models has been called the Holocene "temperature conundrum" (Liu et al., 2014), which was revisited in Wanner (2021), Kaufman et al. (2020) and Kaufman and Broadman (2023). This discrepancy has been attributed to uncertainties in both proxy reconstructions and climate models. One major aspect is the seasonal bias in organic-based proxy records (such as pollen and diatoms) towards summer (Liu et al, 2014). As the Holocene displays opposite trends in summer and winter insolation at 60° N (Fig. 8e, Laskar et al., 2004), high latitudes provide an optimal setting for testing the seasonality aspect in Holocene temperatures. Permafrost ice wedge $\delta^{18}O$, a clear winter season proxy, shows a continuous warming trend in the last 7 kyr BP (Meyer et al., 2015b) that supports the hypothesis that seasonality in proxy-based records is one key variable to be considered. Pollen-based reconstructions for the Holocene show a clear temperature decrease since an early to mid-Holocene temperature optimum (Fig. 8d; Herzschuh et al. 2021, 2022, 2023a, b) that is valid not only for the summer season but (though less pronounced) also for annual reconstructions. Proxy-based reconstructions of Kaufman et al. (2020) also suggest late Holocene cooling. The $\delta^{18}O_{BSi}$ compilation presented here for lacustrine environments is based on diatoms whose bloom is mostly attributed to the late spring–early summer season.

Decreasing summer temperatures throughout the Holocene would manifest in decreasing T_{lake}, which would in turn lead to increasing $\delta^{18}O_{BSi}$ (Fig. 1). The observed decrease in $\delta^{18}O_{BSi}$, however, points towards lower $\delta^{18}O_{lake}$, which would be in line with decreasing $\delta^{18}O_{prec}$ due to decreasing summer T_{air} (Fig. 1). This would imply either a prevalence of summer precipitation or lake basins with sub-annual t_{res}. However, the trend is observed for lake basins with a wide range of t_{res}, suggesting millennial-scale changes in summer T_{air} to be the main driver of the observed $\delta^{18}O_{BSi}$ signal.

It has to be stressed that this influence of T_{air} may act both directly and indirectly: directly by means of the temperature-dependent fractionation during precipitation formation and indirectly via the impact of temperature within the hydrological cycle and $\delta^{18}O$ of water compartments. This includes factors such as moisture origin, precipitation intermittency, and atmospheric circulation patterns, which have been described as key drivers in numerous case studies. This underlines the importance of scale when assessing $\delta^{18}O_{BSi}$ records, both temporally and spatially. On a millennial and hemispheric scale, T_{air} can be identified as one main driver of $\delta^{18}O_{BSi}$ records even though the signal formation is generally complex and challenging to interpret with individual records. A T_{air} influence for certain records on the millennial scale is therefore not necessarily a contradiction to the findings of the original publications that may have attributed the record's signal to other factors (e.g. hydrological processes) on shorter timescales.

4.4 Frontiers and challenges (records older than the Holocene)

Further back in time than the Holocene, coverage with $\delta^{18}O_{BSi}$ records is generally limited. As MIS 1 ($N = 37$) and MIS 2 ($N = 18$) have the highest numbers of records, they offer the best possibility of comparing glacial and interglacial records. Records beyond MIS 2 are very sparse and do not allow for filtering and generating common trends. Here, the in-

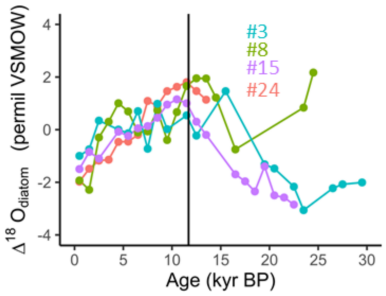

Figure 9. Comparison of MIS 1 and MIS 2 data. Continuation of Holocene records from the NH stack (see Fig. 6f) into MIS 2 for colour-coded records (#3, 8, 15, 24).

terpretation has to rely on comparison of individual datasets. There are few ($N = 16$) records that cross the MIS 1–MIS 2 boundary, and these records cover neither MIS 1 nor MIS 2 entirely. A quantitative comparison of MIS 1 and MIS 2 is therefore difficult. Again, caution has to be applied due to the fact that these records stem from lakes with different hydrological and climatic settings (i.e. maritime Alaskan sites vs. continental Siberian sites).

The most promising approach for investigating MIS 1 and MIS 2 is extending NH MIS 1 datasets to the past (Fig. 9). Five NH $\delta^{18}O_{BSi}$ records (#3, 8, 15, 24, 25) extend back from MIS 1 into MIS 2 and offer insight into the hydroclimate history of Siberia during the last glacial and the deglaciation. Four of these records (#3, 8, 15, 24) are continuations of records included in the NH stack (see Fig. 6f), and all of them stem from Asia. Most records display a maximum near the MIS 1–MIS 2 boundary and a decrease in $\delta^{18}O_{BSi}$ with increasing age in MIS 2, suggesting decreasing T_{air}. This is the case for all records except #3, which displays a relative $\delta^{18}O_{BSi}$ maximum at ca. 16 kyr BP. This maximum may also be caused by dry conditions outperforming the effect of lower T_{air}. Only records #3, #8, and #15 extend beyond 13 kyr BP. Both #3 and #15 reach their absolute minima at 23 and 24 kyr BP, respectively. Record #8 does not show such a clear pattern and shows a relative maximum at 25 kyr BP instead. This is likely due to the complex hydrological setting (alternating between open and closed at present) which may have changed over these timescales. Generally, most records suggest a tendentially lower $\delta^{18}O_{BSi}$ in MIS 2 when compared to MIS 1.

This is notable as glacial and interglacial periods are characterized by different environments, atmospheric circulation patterns, and likely hydrological settings (e.g. formation or closure of outflows from lakes, lake level fluctuations). Potentially, lower $\delta^{18}O_{BSi}$ values would be consistent with either lower T_{air} or more humid conditions. In the case of MIS2, generally associated with cold and dry conditions, a lower T_{air} is the more plausible scenario. However, it must be stressed that the lack of records covering the complete MIS 2 complicates a robust statistical comparison between MIS 1 and 2. Calculated offsets of MIS 1 and MIS 2 data points may show both higher and lower $\delta^{18}O_{BSi}$ values in MIS 2 compared to the Holocene. Again, a MIS 2 climate colder and drier than Holocene (MIS 1) may produce either lower or higher $\delta^{18}O_{BSi}$ values due to opposing effects of T_{air} and evaporation. A geographical pattern of either of these effects prevailing is not obvious, which suggests that rather than the climatic background, the individual hydrological settings of the lakes play a prominent role in determining the $\delta^{18}O_{BSi}$ signal. This supports the approach of using lakes with both similar latitudinal and hydrological characteristics for meaningful inter-site comparison.

Beyond MIS 2, $\delta^{18}O_{BSi}$ records become even scarcer, as do lake sediment records in general. Additionally, lake sediments covering these time periods often lack sufficient diatoms, especially in cold stages, i.e. Lake Baikal during MIS 4 (Mackay et al., 2008; Mackay et al., 2011; Mackay et al., 2013).

Lake El'gygytgyn is a peculiar example of a continuous sedimentation history, with $\delta^{18}O_{BSi}$ showing glacial–interglacial cycles at least back to MIS 9 (Chapligin et al., 2012b), which have been attributed by the authors to T_{air} changes. In addition to glacial–interglacial cycles, it is also possible to compare $\delta^{18}O_{BSi}$ of interglacials, i.e. MIS 1, MIS 5, MIS 11, when diatoms during cold stages are absent. In the sedimentary records of Lake El'gygytgyn, Chapligin et al. (2012c) investigated the $\delta^{18}O_{BSi}$ differences between the warm stages MIS 1, MIS 5, and MIS 11 and found MIS 11 as warmest interglacial. This interpretation has been supported by pollen-based T_{air} reconstructions by Melles et al. (2012) and underlines the applicability of the $\delta^{18}O_{BSi}$ proxy on glacial–interglacial timescales. Long-term diagenetic effects have shown to be of little influence on $\delta^{18}O_{BSi}$, at least for the last 250 kyr (Chapligin et al., 2012b). Studies on Lake Baikal have also investigated past interglacials and have addressed changes in precipitation intermittency and cooling events during MIS 11 (Mackay et al., 2008). During MIS 5, millennial-scale variability is suggested to have been more stable than during MIS 1 (Mackay et al., 2013).

Older $\delta^{18}O_{BSi}$ records do exist and often rely on paleolakes, i.e. Ribains Maar, Baringo–Bogoria basin, Makgadikgadi, and Dethlingen (Shemesh et al., 2001b; Koutsodendris et al., 2012; Wilson et al., 2014b; Schmidt et al., 2017). These offer the possibility of extending the picture past extant lakes. However, the absence of modern hydrological observations makes their interpretation and comparison to other, better-constrained records more challenging. Further research using $\delta^{18}O_{BSi}$ is therefore needed in order to complement the picture and provide insight into past climate and environmental conditions in continental regions, particularly valuable for high-latitude and high-altitude areas that are poorly covered by other proxy data. We recommend studies with uniform spatial and temporal coverage, i.e. hydrologically open lakes with a long, continuous sedimentation history, as our synthesis indicates these to be most promising for generating com-

parable binned time series to extend climate reconstructions further into the past.

5 Conclusions

In this study, we have identified and compiled all existing lacustrine $\delta^{18}O_{BSi}$ records published to date and synthesized them into the first global $\delta^{18}O_{BSi}$ data compilation. We have identified 53 $\delta^{18}O_{BSi}$ records derived from 71 publications. These records stem from across the entire globe with their geographical distribution focusing on high-altitude and high-latitude lacustrine environments. Diatoms bear the advantage of being available in dilute, non-alkaline lakes common in these environments. Regional clusters of records (e.g. northern Eurasia, eastern Africa) indicative of the research foci of the individual research groups employing the $\delta^{18}O_{BSi}$ proxy allow for generating regional subsets of data. Temporal coverage stretches from sub-recent timescales to the Pliocene, which highlights the applicability of $\delta^{18}O_{BSi}$ on different timescales. Best coverage is available in the Holocene (MIS 1), which is linked to the age of lakes and hence the availability of lake sediments, especially at high latitudes. Moreover, biogenic silica (here entirely from diatom-based samples) is most abundant during warm periods (interstadials and interglacials) compared to colder periods. The interpretability of $\delta^{18}O_{BSi}$ records relies on regional setting and hydrological constraints of individual lakes and catchments and is preferably supported by isotope measurements of modern lake water. Most $\delta^{18}O_{BSi}$ records stem from open lakes ($N = 41$), suggesting for these lakes a negligible influence of lake evaporation. In contrast, closed lakes ($N = 12$) and paleo-lakes ($N = 9$) have been investigated less. It has to be noted that a lake's ontogeny and hydrology may change throughout time, and thus hydrological changes constitute a valid approach for interpreting these $\delta^{18}O_{BSi}$ records.

Spatial resolution of the $\delta^{18}O_{BSi}$ records is determined by the size of the lake and its corresponding catchment with lake water effectively integrating the input signal. While this signal may integrate large areas such as at Lake Baikal, most catchments ($N = 18$) are $< 100\,km^2$, suggesting a locally confined signal for these lakes. Regarding temporal resolution, most records feature sampling resolutions which by far exceed t_{res}, suggesting sampling resolution to be the decisive factor in determining a record's signal. However, in case of $t_{res} > 100\,yr$, lakes may be subject to increased lake evaporation.

Accounting for offsets and different temporal resolution of records and filtering for similar hydrological settings (hydrologically open lakes with $t_{res} < 100\,yr$), we find a common pattern throughout the Common Era at the centennial scale, which we attribute to changing hydroclimate conditions. Changes are similar between Eurasia and North America, but they still differ in the timing of $\delta^{18}O_{BSi}$ maxima. Generally, the combined Eurasian $\delta^{18}O_{BSi}$ record seems to include major climate episodes during this period, including Roman Climate Optimum, Migration Period Pessimum, Medieval Climatic Anomaly (MCA), and Little Ice Age. An effect of recent warming is not visible in the Common Era data.

For the entire Holocene in Eurasia and the NH (for hydrologically open lakes with $t_{res} < 100\,yr$), we find a common decreasing $\delta^{18}O_{BSi}$ trend of ca. $-0.2\,‰\,kyr^{-1}$ on the millennial scale which roughly follows summer insolation. The decreasing $\delta^{18}O_{BSi}$ trend is accelerated in the second half of the Holocene, thus in Neoglacial times. Hence, this summer-based proxy contributes to the understanding of the Holocene climate history and the Holocene conundrum discussion initiated by Liu et al. (2014). The timing of the absolute $\delta^{18}O_{BSi}$ maxima of individual records in Eurasia differs and shows an east–west gradient with eastern Eurasian records featuring earlier Holocene maxima compared to western Eurasian records. Holocene minima occur within the last 2 kyr for all Eurasian records. North American records diverge from this Holocene pattern with later maxima and earlier minima. This behaviour is likely linked to atmospheric circulation patterns as also described by the authors of the individual records.

Extending the millennial-scale trend of Eurasian records into MIS 2 shows generally lower $\delta^{18}O_{BSi}$ values in MIS 2, suggesting lower T_{air} (and not P/E) in glacial times, also visible in most other records that act on glacial–interglacial timescales. The applicability of the $\delta^{18}O_{BSi}$ proxy beyond MIS 2 is generally constrained by the availability of lake sediments and the abundance of diatoms in the respective sediments. Lake El'gygytgyn, as a prime example of hydrological continuity, displays glacial–interglacial cycles in the $\delta^{18}O_{BSi}$ record, supporting T_{air} being a prominent driver of $\delta^{18}O_{BSi}$ on millennial timescales. In glacial periods, diatoms abundances are low, and this limitation sometimes does not allow for $\delta^{18}O_{BSi}$ analysis. However, comparison between interglacials where diatoms are generally more abundant is feasible, i.e. at Lake Baikal and Lake El'gygytgyn. In summary, we demonstrate the applicability and inter-comparability of combined $\delta^{18}O_{BSi}$ records into a first lacustrine $\delta^{18}O_{BSi}$ compilation allowing for paleoclimate reconstructions and accounting for regional offsets, different temporal resolutions, and hydrological backgrounds. $\delta^{18}O_{BSi}$ records compiled in this study are an important tool for reconstructing paleoclimate across the globe and across a variety of timescales. In NH extratropical regions, their T_{air}-driven quantitative signal makes them especially useful in conjunction with paleoclimate models. Future research would be most valuable in complementing the existing data with longer records (covering MIS 2 and beyond) and records from underrepresented regions such as the Southern Hemisphere.

Appendix A

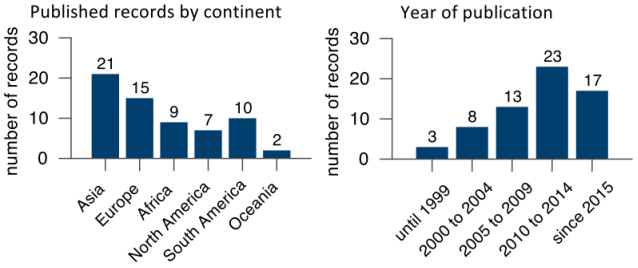

Figure A1. Geographical distribution of published $\delta^{18}O_{BSi}$ records and year of publication ($N = 64$).

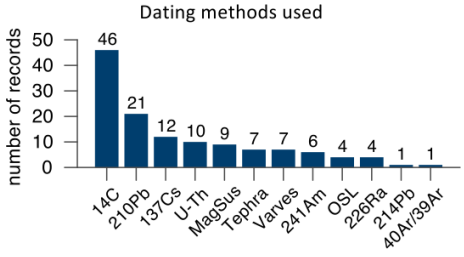

Figure A2. Overview of the dating methods used for age model creation of published $\delta^{18}O_{BSi}$ time series ($N = 64$). Note that a single record can rely on multiple methods.

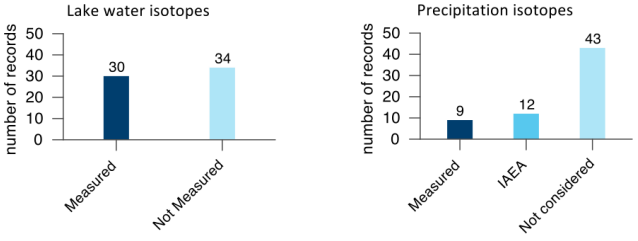

Figure A3. Overview of isotope hydrological background information considered in publications presenting $\delta^{18}O_{BSi}$ records ($N = 64$).

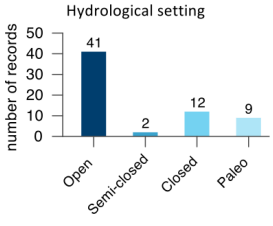

Figure A4. Hydrological settings of the lakes corresponding to the $\delta^{18}O_{BSi}$ records compiled in this study, as indicated in the original publications ($N = 64$). Owing to a lack of present constraints, paleolakes are listed as a separate category.

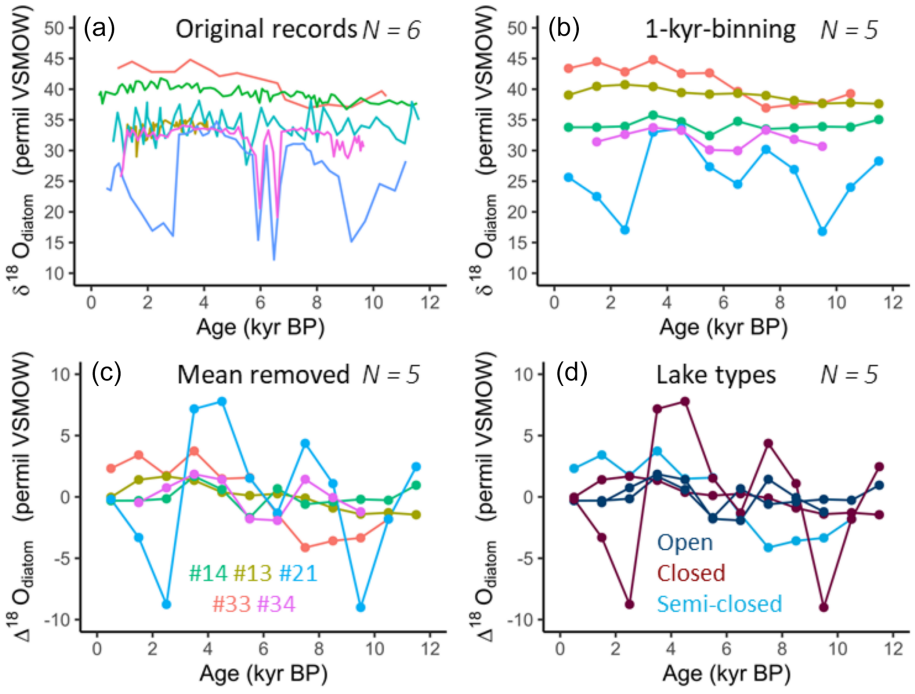

Figure A5. Holocene $\delta^{18}O_{BSi}$ dataset for the African continent. **(a)** Original records, **(b)** data binned to 1 kyr intervals only showing records covering at least seven bins, **(c)** binned records with the mean of individual records removed, **(d)** with data including hydrological background information.

Table A1. Overview of the records and corresponding publications identified by this study (single meaning single core; composite meaning several cores; supplemented meaning information from other publication added, e.g. the age model).

Rec_ID	Archive	Lake	Core type	original Core ID	Field campaign (Year)	Short reference	Used for record number
EC1	Paleolake	Les Echets	single	EC1	2001	Ampel et al. (2009)	#12
HL1	Lake	Heart Lake	composite	10-AS-1D; 09-AS-1A; 09-AS-1B	2009, 2010	Bailey et al. (2018)	#35
LCHA1	Lake	Lake Challa	composite	03-2K; 05-4P	2003	Barker et al. (2011)	#13
M982P	Lake	Lake Malawi	single	M98-2P	1998	Barker et al. (2007)	#14
SHT1	Lake	Small Hall Tarn			1996	Barker et al. (2001)	#21
ST1	Lake	Simba Tarn			1996	Barker et al. (2001)	#34
BALGGU171	Lake	Garba Guracha	composite	BAL-GGU17-1A; BAL-GGU17-1B	2017	Bittner et al. (2021)	#33
SCP162A	Lake	Schrader Pond	single	SCP16-2A	2016	Broadman et al. (2020a)	#39
SILMC	Lake	Sunken Island Lake	composite	SIL-MC	2017	Broadman et al. (2020b)	#26
YL16-2C	Lake	Yellowstone Lake	composite	YL16-2C-1K; YL17-13A-1G	2016	Brown et al. (2021)	#53
PET09P2	Lake	Lac Petit	single	PET09P2	2009	Cartier et al. (2019b)	#44
Ni2B	Lake	Nettilling Lake	supplemented	Ni-2B	2012	Chapligin et al. (2016a)	#41
Lz1024	Lake	El'gygytgyn	single	Lz1024	2003	Chapligin et al. (2012b)	#3
LALB94	Lake	Lake Albano	supplemented	6A, 6B	1994	Chondrogianni et al. (2004)	–
NAR0110	Lake	Nar Gölü	single	NAR01/02	2001	Dean et al. (2018)	#23
NAR0110	Lake	Nar Gölü	single	NAR10	2010	Dean et al. (2018)	#23
BNT1418	Lake	Baunt Lake	composite	BNT14	2014	Harding et al. (2020)	#25
LG1	Lake	Lago Chungara	composite	10; 11	2002	Hernandez et al. (2011)	#28
LCHUN02	Lake	Lago Chungara	composite	10; 11	2002	Hernandez et al. (2008)	#28
LG1	Lake	Lago Chungara	composite	10; 11	2002	Hernandez et al. (2013)	#28
LCHUN02	Lake	Lago Chungara	composite	10; 11	2002	Hernandez et al. (2010)	#28
P2	Lake	Lake Pupuke	single	P2	2001	Heyng et al. (2015)	#42
GL1	Lake	Grandfather Lake	single			Hu and Shemesh (2003)	#27
ARL1	Lake	Arolik Lake				Hu et al. (2003)	–
LCHUN96	Lake	Lake Chuna	composite		1996	Jones et al. (2004)	#38
SS1	Lake	Lake Spaime	single	SS1	2002	Jonsson et al. (2010)	#49
VA	Lake	Vuolep Allakasjaure	supplemented	VAY1	2006	Jonsson et al. (2010)	#43
LB0301	Lake	Lake Baikal	single	03-01		Kalmychkov et al. (2007)	#9
LB0402	Lake	Lake Baikal	single	04-02		Kalmychkov et al. (2007)	#10
Co1412	Lake	Lake Emanda	single	Co 1412	2017	Kostrova et al. (2021)	#24
Co1309	Lake	Lake Ladoga	single	Co 1309	2013	Kostrova et al. (2019)	#31
KTK2	Lake	Kotokel Lake	single	KTK2	2005	Kostrova et al. (2013a)	#8
KTK2	Lake	Kotokel Lake	single	KTK2	2005	Kostrova et al. (2013b)	#8
KTK2	Lake	Kotokel Lake	single	KTK2	2005	Kostrova et al. (2014)	#8
KTK2	Lake	Kotokel Lake	single	KTK2	2005	Kostrova et al. (2016)	#8
D1	Paleolake	Dethlingen	single		2004	Koutsodendris et al. (2012)	#52
LT1	Lake	Lake Tilo	composite	T97; T95	1995	Lamb et al. (2005)	#40
PN94C	Lake	Lake Pinarbasi	single	PN94C	1994	Leng et al. (2001)	#7
ZAC3	Lake	Laguna Zacapu	single	ZAC/3	2001	Leng et al. (2005)	#47
ZK2	Lake	Laguna Zacapu	single	ZK2	2001	Leng et al. (2005)	#50
BDP962	Lake	Lake Baikal	single	BDP-96-2	1996	Mackay et al. (2008)	#2
CON016053	Lake	Lake Baikal	supplemented	CON01-605-3	2001	Mackay et al. (2011)	#20
CON016032	Lake	Lake Baikal	single	CON-01-603-2	2001	Mackay et al. (2013)	#4
TDB1	Lake	Lake Brazi	single	TDB-1	2007	Magyari et al. (2013)	#22
Co1321	Lake	Bolshoye Shchuchye	single	Co1321	2016	Meyer et al. (2022)	#16
PG1857	Lake	Two-Yurts Lake	composite	PG1857; PG1857-2	2007	Meyer et al. (2015a)	#45
CON016053	Lake	Lake Baikal	supplemented	CON01-605-3	2001	Morley et al. (2005)	–
LVA1	Lake	Laguna Verde Alta	composite			Polissar et al. (2006)	#32
LVB1	Lake	Laguna Verda Baja	supplemented			Polissar et al. (2006)	#18
PTAU1	Paleolake	Tauca	supplemented	BT		Quesada et al. (2015)	#17
PTAU1	Paleolake	Tauca	supplemented	CB		Quesada et al. (2015)	#17
PTAU1	Paleolake	Tauca	supplemented	EWK		Quesada et al. (2015)	#17
PTAU1	Paleolake	Tauca	supplemented	PJ		Quesada et al. (2015)	#17
HT1	Lake	Hausberg Tarn			1996	Rietti-Shati et al. (1998)	#46
VA	Lake	Vuolep Allakasjaure	supplemented	VA2	2000	Rosqvist et al. (2004)	#43
LS1	Lake	Lake Spaime	supplemented	Core III	2006	Rosqvist et al. (2013)	#49
LSG1	Lake	Lake Stuor Goussasjavri	supplemented	Core III	2007	Rosqvist et al. (2013)	#48
TL1	Lake	Tonsberg Lake	composite		1991	Rosqvist et al. (1999)	#19
G702	Lake	Lake Gosciaz	supplemented	G7/02	2002	Rozanski et al. (2010)	#29
MC2	Lake	Mica Lake	supplemented	MC-2	2006	Schiff et al. (2009)	#36
MBG1	Paleolake	Makgadikgadi	outcrop		2011	Schmidt et al. (2017)	#6
RM1	Paleolake	Ribains Maar	single		1988	Shemesh et al. (2001b)	#5
LP1	Lake	Linsley Pond	supplemented		1987	Shemesh and Peteet (1998)	#30
L850	Lake	Lake 850	single		1999	Shemesh et al. (2001a)	#37
R1	Lake	Lake Rutundu	single	R-1	1996	Street-Perrott et al. (2008)	#11
BAIK13	Lake	Lake Baikal	single	BAIK13-1	2013	Swann et al. (2018)	#51
BAIK13	Lake	Lake Baikal	single	BAIK13-4	2013	Swann et al. (2018)	#51
BAIK13	Lake	Lake Baikal	single	BAIK13-5	2013	Swann et al. (2018)	#51
BAIK13	Lake	Lake Baikal	single	BAIK13-7	2013	Swann et al. (2018)	#51
Lz1029	Lake	El'gygytgyn	composite	Lz1029	2003	Swann et al. (2010)	#15
BD4	Paleolake	Baringo-Bogoria Basin	outcrop	BD_4		Wilson et al. (2014b)	#1

Table A2. Overview of the records compiled and analysed in this study. Lake basin parameters shown are taken from the HydroLakes database (Messager et al., 2016) for consistency. In case of major discrepancies between the HydroLakes database and the values provided by individual case studies, values of case are given as well and marked with an asterisk.

No.	Archive	Lake	Short reference	Lat. (dec deg)	Long. (dec deg)	Water depth (m)	Altitude (m a.s.l.)	Lake area (km^2)	Catchment area (km^2)	Residence time (a)	Chron.	Rec_ID
#1	Paleolake	Baringo-Bogoria Basin	Wilson et al. (2014b)	0.55	35.94		1178				Y	BD4
#2	Lake	Baikal	Mackay et al. (2008)	53.70	108.35	321	449	31 968	569 176	375	Y	BDP962
#3	Lake	El'gygytgyn	Chapligin et al. (2012b)	67.50	172.08	170	471	119	292	64	Y	Lz1024
#4	Lake	Baikal	Mackay et al. (2013)	53.96	108.91	386	449	31 968	569 176	375	Y	CON01 6032
#5	Paleolake	Ribains Maar	Shemesh et al. (2001b)	44.84	3.82		1074				N	RM1
#6	Paleolake	Makgadikgadi	Schmidt et al. (2017)	−20.29	24.27		934				N	MBG1
#7	Lake	Lake Pinarbasi	Leng et al. (2001)	37.47	33.12		1000	0.002			Y	PN94C
#8	Lake	Kotokel Lake	Kostrova et al. (2013a, b, 2014, 2016)	52.78	108.12	4	453	65.7	170	58	Y	KTK2
#9	Lake	Baikal	Kalmychkov et al. (2007)	53.75	108.41	348	449	31 968	569 176	375	N	LB0301
#10	Lake	Baikal	Kalmychkov et al. (2007)	53.39	107.53	233	449	31 968	569 176	375	N	LB0402
#11	Lake	Lake Rutundu	Street-Perrott et al. (2008)	−0.03	37.45	11	3078	0.40			Y	R1
#12	Paleolake	Les Echets	Ampel et al. (2009)	45.90	4.93		267				Y	EC1
#13	Lake	Lake Challa	Barker et al. (2011)	−3.32	37.42	94	878	4.12	6.4	86	Y	LCHA1
#14	Lake	Lake Malawi	Barker et al. (2007)	−9.98	34.23	363	476	29 544	128 727	219	Y	M982P
#15	Lake	El'gygytgyn	Swann et al. (2010)	67.66	172.14	177.0	471	119	292	64	Y	Lz1029
#16	Lake	Bolshoye Shchuchye	Meyer et al. (2022)	67.88	66.32	132.0	186	11.80	227	5	Y	Co1321
#17	Paleolake	Tauca	Quesada et al. (2015)	−19.16	−68.20		3685				Y	PTAU1
#18	Lake	Laguna Verda Baja	Polissar et al. (2006)	8.86	−70.87	5	4170				Y	LVB1
#19	Lake	Tonsberg Lake	Rosqvist et al. (1999); Rosqvist, Rietti-Shati, and Shemesh (1999)	−54.17	−36.69		70	0.01			Y	TL1
#20	Lake	Baikal	Mackay et al. (2011)	51.58	104.85	600.0	449	31 968	569 176	375	Y	CON01 6053
#21	Lake	Small Hall Tarn	Barker (2001)	−0.15	37.35		4289				Y	SHT1
#22	Lake	Lake Brazi	Magyari et al. (2013)	45.40	22.90	1.1	1740	0.004	0.10	0.5	Y	TDB1
#23	Lake	Nar Gölü	Dean et al. (2018)	38.34	34.46	25.0	1369	0.52	3.5	15	Y	NAR0110
#24	Lake	Lake Emanda	Kostrova et al. (2021)	65.28	135.75	14.6	654	33.10	118	26	Y	Co1412
#25	Lake	Baunt Lake	Harding et al. (2020)	55.19	113.03	33	1052	112	10 256	1.1	Y	BNT1418
#26	Lake	Sunken Island Lake	Broadman et al. (2020b)	60.59	−150.89	7	84	0.44	28.3	0.18	Y	SILMC
#27	Lake	Grandfather Lake	Hu and Shemesh (2003)	60.80	−158.52	20	142	0.35			Y	GL1
#28	Lake	Lago Chungara	Hernandez et al. (2008, 2010, 2011, 2013)	−18.25	−69.17	40	4556	21.27	265	289 (15*)	Y	LG1
#29	Lake	Lake Gosciaz	Rozanski et al. (2010)	52.58	19.35	25	63	0.38	20.6	0.51	Y	G702
#30	Lake	Linsley Pond	Shemesh and Peteet (1998)	41.30	−72.75	9	8	0.93			Y	LP1
#31	Lake	Lake Ladoga	Kostrova et al. (2019)	60.98	30.68	111		17 444	279 581	11	Y	Co1309
#32	Lake	Laguna Verde Alta	Polissar et al. (2006)	8.85	−70.87	3	4215				Y	LVA1
#33	Lake	Garba Guracha	Bittner et al. (2021)	6.88	39.88	5	3950	0.15	0.15		Y	BALGGU171
#34	Lake	Simba Tarn	Barker (2001)	−0.15	37.32		4959	0.00			Y	ST1
#35	Lake	Heart Lake	Bailey et al. (2018)	51.85	−176.69	7.6	60	0.25	8	0.038	Y	HL1
#36	Lake	Mica Lake	Schiff et al. (2009)	60.96	−148.15	58	93	0.63	3.2	0.46	Y	MC2
#37	Lake	Lake 850	Shemesh et al. (2001a)	68.25	19.12	8	850		0.5		Y	L850
#38	Lake	Lake Chuna	Jones et al. (2004)	67.95	32.48		475	0.13	2	0.30	Y	LC1
#39	Lake	Schrader Pond	Broadman et al. (2020a)	69.36	−145.08		869				Y	SCP162A
#40	Lake	Lake Tilo	Lamb et al. (2005)	7.06	38.10	10	1551	0.66	144	0.15	Y	LT1
#41	Lake	Nettilling Lake	Chapligin et al. (2016b); Narancic et al. (2016)	66.50	−70.50	14	18	4872.70	63 400	5.5	N	Ni2B
#42	Lake	Lake Pupuke	Heyng et al. (2015)	−36.78	174.77	58	11	1.01	1	5.8	Y	P210/P260
#43	Lake	Vuolep Allakasjaure	Jonsson et al. (2010)	68.18	18.17	11	991	1.01	1	5.8	Y	VA
#44	Lake	Lac Petit	Cartier et al. (2019a)	44.11	7.19	7	2200	0.018	6		Y	PET09P2
#45	Lake	Two-Yurts Lake	Meyer et al. (2015a)	56.82	160.11	28	264	0.02	6		Y	PG1857
#46	Lake	Hausberg Tarn	Rietti-Shati et al. (1998)	−0.15	37.30		4369	11.39	206	1.9	Y	
#47	Lake	Laguna Zacapu	Leng et al. (2005)	19.83	−101.79	2.0	1987	0.23	66	0.037	N	ZAC3
#48	Lake	Lake Stuor Goussasjavri	Rosqvist et al. (2013)	67.85	19.68	6	559	0.28	0.5	5.6	Y	LSG1
#49	Lake	Lake Spaime	Rosqvist et al. (2013)	63.12	12.32	4	887	0.03	3.5	0.04	Y	LS1
#50	Lake	Laguna Zacapu	Leng et al. (2005)	19.82	−101.79	8	1987	0.23	66	0.037	N	ZK2
#51	Lake	Baikal	Swann et al. (2018)	51.77	104.42	1360	449	31 968	569 176	375	Y	BAIK13
#52	Paleolake	Dethlingen	Koutsodendris et al. (2012)	52.96	10.14		65				N	D110
#53	Lake	Yellowstone Lake	Brown et al. (2021)	44.54	−110.39	61	2360	340	2579	21 (14*)	Y	YL16-2C

Data availability. The dataset is being submitted to PANGAEA and will be available from the following link after publication: https://doi.pangaea.de/10.1594/PANGAEA.957160 (Meister et al., 2024).

Author contributions. PM, HM, BD, and BB designed the research project and the structure of the manuscript. PM compiled the database, carried out statistical analyses, produced all figures and tables, and wrote the main part of the manuscript. ML, GR, AH, GS, AM, HM, HB, and PB contributed data that were not publicly available. All co-authors brought in their expertise made substantial contributions to the manuscript. All authors wrote parts of the manuscript, commented on drafts, and approved the final submitted version.

Competing interests. The contact author has declared that none of the authors has any competing interests.

Disclaimer. Maps throughout this article were created using ArcGIS® software by Esri. ArcGIS® and ArcMap™ are the intellectual property of Esri and are used herein under license. Copyright © Esri. All rights reserved. For more information about Esri® software, please visit https://www.esri.com/en-us/home (last access: August 2022).

Publisher's note: Copernicus Publications remains neutral with regard to jurisdictional claims made in the text, published maps, institutional affiliations, or any other geographical representation in this paper. While Copernicus Publications makes every effort to include appropriate place names, the final responsibility lies with the authors.

Acknowledgements. We thank Heinz Wanner, Witold Bagniewski, and one anonymous reviewer, whose comments helped substantially improving the paper. We also thank all scientists and technicians developing and advancing the research field of oxygen isotopes in diatom silica.

Financial support. Philip Meister has been funded by Bundesministerium für Bildung, Wissenschaft, Forschung und Technologie via the Palmod2 project (grant no. 01LP1923B). Hannah Bailey has been funded by the Academy of Finland (grant no. 348536). Armand Hernandez has been funded by the Spanish Ministry of Science and Innovation through the Ramón y Cajal Scheme (RYC2020-029253-I).

The article processing charges for this open-access publication were covered by the Alfred-Wegener-Institut Helmholtz-Zentrum für Polar- und Meeresforschung.

Review statement. This paper was edited by Denis-Didier Rousseau and reviewed by Witold Bagniewski, Heinz Wanner, and one anonymous referee.

References

Akse, S. P., Polerecky, L., Kienhuis, M. V. M., and Middelburg, J. J.: The influence of sediment diagenesis and aluminium on oxygen isotope exchange of diatom frustules, Geochim. Cosmochim. Ac., 333, 362–372, https://doi.org/10.1016/j.gca.2022.07.015, 2022.

Ampel, L., Wohlfarth, B., Risberg, J., Veres, D., Leng, M. J., and Tillman, P. K.: Diatom assemblage dynamics during abrupt climate change: the response of lacustrine diatoms to Dansgaard–Oeschger cycles during the last glacial period, J. Paleolimnol., 44, 397–404, https://doi.org/10.1007/s10933-009-9350-7, 2009.

Andersen, K. K., Azuma, N., Barnola, J. M., Bigler, M., Biscaye, P., Caillon, N., Chappellaz, J., Clausen, H. B., Dahl-Jensen, D., Fischer, H., Flückiger, J., Fritzsche, D., Fujii, Y., Goto-Azuma, K., Grønvold, K., Gundestrup, N. S., Hansson, M., Huber, C., Hvidberg, C. S., Johnsen, S. J., Jonsell, U., Jouzel, J., Kipfstuhl, S., Landais, A., Leuenberger, M., Lorrain, R., Masson-Delmotte, V., Miller, H., Motoyama, H., Narita, H., Popp, T., Rasmussen, S. O., Raynaud, D., Rothlisberger, R., Ruth, U., Samyn, D., Schwander, J., Shoji, H., Siggard-Andersen, M. L., Steffensen, J. P., Stocker, T., Sveinbjörnsdóttir, A. E., Svensson, A., Takata, M., Tison, J. L., Thorsteinsson, T., Watanabe, O., Wilhelms, F., White, J. W. C., and North Greenland Ice Core Project, m.: High-resolution record of Northern Hemisphere climate extending into the last interglacial period, Nature, 431, 147–151, https://doi.org/10.1038/nature02805, 2004.

Bailey, H. L., Kaufman, D. S., Henderson, A. C., and Leng, M. J.: Synoptic scale controls on the $\delta^{18}O$ in precipitation across Beringia, Geophys. Res. Lett., 42, 4608–4616, https://doi.org/10.1002/2015GL063983, 2015.

Bailey, H. L., Kaufman, D. S., Sloane, H. J., Hubbard, A. L., Henderson, A. C. G., Leng, M. J., Meyer, H., and Welker, J. M.: Holocene atmospheric circulation in the central North Pacific: A new terrestrial diatom and $\delta^{18}O$ dataset from the Aleutian Islands, Quaternary Sci. Rev., 194, 27–38, https://doi.org/10.1016/j.quascirev.2018.06.027, 2018.

Barker, P. A.: A 14,000-Year Oxygen Isotope Record from Diatom Silica in Two Alpine Lakes on Mt. Kenya, Science, 292, 2307–2310, https://doi.org/10.1126/science.1059612, 2001.

Barker, P. A., Street-Perrott, F. A., Leng, M. J., Greenwood, P. B., Swain, D. L., Perrott, R. A., Telford, R. J., and Ficken, K. J.: A 14,000-year oxygen isotope record from diatom silica in two alpine lakes on Mt. Kenya, Science, 292, 2307–2310, https://doi.org/10.1126/science.1059612, 2001.

Barker, P. A., Leng, M. J., Gasse, F., and Huang, Y.: Century-to-millennial scale climatic variability in Lake Malawi revealed by isotope records, Earth Planet. Sc. Lett., 261, 93–103, https://doi.org/10.1016/j.epsl.2007.06.010, 2007.

Barker, P. A., Hurrell, E. R., Leng, M. J., Wolff, C., Cocquyt, C., Sloane, H. J., and Verschuren, D.: Seasonality in equatorial climate over the past 25 k.y. revealed by oxygen isotope records from Mount Kilimanjaro, Geology, 39, 1111–1114, https://doi.org/10.1130/g32419.1, 2011.

Biskaborn, B. K., Subetto, D. A., Savelieva, L. A., Vakhrameeva, P. S., Hansche, A., Herzschuh, U., Klemm, J., Heinecke, L., Pestryakova, L. A., Meyer, H., Kuhn, G., and Diekmann, B.: Late Quaternary vegetation and lake system dynamics in north-eastern Siberia: Implications for seasonal climate variability, Quaternary Sci. Rev., 147, 406–421, https://doi.org/10.1016/j.quascirev.2015.08.014, 2016.

Bittner, L., Gil-Romera, G., Grady, D., Lamb, H. F., Lorenz, E., Weiner, M., Meyer, H., Bromm, T., Glaser, B., and Zech, M.: The Holocene lake-evaporation history of the afro-alpine Lake Garba Guracha in the Bale Mountains, Ethiopia, based on $\delta^{18}O$ records of sugar biomarker and diatoms, Quaternary Res., 105, 23–36, https://doi.org/10.1017/qua.2021.26, 2021.

Bowen, G. J.: The Online Isotopes in Precipitation Calculator version OIPC3.1, http://www.waterisotopes.org (last access: August 2022), 2022.

Bradley, R. S., Hughes, M. K., and Diaz, H. F.: Climate in Medieval Time, Science, 302, 404–405, https://doi.org/10.1126/science.1090372, 2003.

Brewer, T. S., Leng, M. J., Mackay, A. W., Lamb, A. L., Tyler, J. J., and Marsh, N. G.: Unravelling contamination signals in biogenic silica oxygen isotope composition: the role of major and trace element geochemistry, J. Quaternary Sci., 23, 321–330, https://doi.org/10.1002/jqs.1171, 2008.

Broadman, E., Kaufman, D. S., Henderson, A. C. G., Malmierca-Vallet, I., Leng, M. J., and Lacey, J. H.: Coupled impacts of sea ice variability and North Pacific atmospheric circulation on Holocene hydroclimate in Arctic Alaska, P. Natl. Acad. Sci. USA, 117, 33034–33042, https://doi.org/10.1073/pnas.2016544117, 2020a.

Broadman, E., Kaufman, D. S., Henderson, A. C. G., Berg, E. E., Anderson, R. S., Leng, M. J., Stahnke, S. A., and Muñoz, S. E.: Multi-proxy evidence for millennial-scale changes in North Pacific Holocene hydroclimate from the Kenai Peninsula lowlands, south-central Alaska, Quaternary Sci. Rev., 241, 106420, https://doi.org/10.1016/j.quascirev.2020.106420, 2020b.

Brown, S. R., Cartier, R., Schiller, C. M., Zahajská, P., Fritz, S. C., Morgan, L. A., Whitlock, C., Conley, D. J., Lacey, J. H., Leng, M. J., and Shanks, W. C. P.: Multi-proxy record of Holocene paleoenvironmental conditions from Yellowstone Lake, Wyoming, USA, Quaternary Sci. Rev., 274, 107275, https://doi.org/10.1016/j.quascirev.2021.107275, 2021.

Büntgen, U., Myglan, V. S., Ljungqvist, F. C., McCormick, M., Di Cosmo, N., Sigl, M., Jungclaus, J., Wagner, S., Krusic, P. J., Esper, J., Kaplan, J. O., de Vaan, M. A. C., Luterbacher, J., Wacker, L., Tegel, W., and Kirdyanov, A. V.: Cooling and societal change during the Late Antique Little Ice Age from 536 to around 660 AD, Nat. Geosci., 9, 231–236, https://doi.org/10.1038/ngeo2652, 2016.

Cartier, R., Sylvestre, F., Paillès, C., Sonzogni, C., Couapel, M., Alexandre, A., Mazur, J.-C., Brisset, E., Miramont, C., and Guiter, F.: Diatom-oxygen isotope record from high-altitude Lake Petit (2200 m a.s.l.) in the Mediterranean Alps: shedding light on a climatic pulse at 4.2 ka, Clim. Past, 15, 253–263, https://doi.org/10.5194/cp-15-253-2019, 2019a.

Cartier, R., Sylvestre, F., Paillès, C., Sonzogni, C., Couapel, M., Alexandre, A., Mazur, J.-C., Brisset, E., Miramont, C., and Guiter, F.: Diatom-oxygen isotope record from high-altitude Lake Petit (2200 m a.s.l.) in the Mediterranean Alps: shedding light on a climatic pulse at 4.2 ka, Clim. Past, 15, 253–263, https://doi.org/10.5194/cp-15-253-2019, 2019b.

Chapligin, B., Leng, M. J., Webb, E., Alexandre, A., Dodd, J. P., Ijiri, A., Lücke, A., Shemesh, A., Abelmann, A., Herzschuh, U., Longstaffe, F. J., Meyer, H., Moschen, R., Okazaki, Y., Rees, N. H., Sharp, Z. D., Sloane, H. J., Sonzogni, C., Swann, G. E. A., Sylvestre, F., Tyler, J. J., and Yam, R.: Interlaboratory comparison of oxygen isotope compositions from biogenic silica, Geochim. Cosmochim. Ac., 75, 7242–7256, https://doi.org/10.1016/j.gca.2011.08.011, 2011.

Chapligin, B., Meyer, H., Bryan, A., Snyder, J., and Kemnitz, H.: Assessment of purification and contamination correction methods for analysing the oxygen isotope composition from biogenic silica, Chem. Geol., 300, 185–199, https://doi.org/10.1016/j.chemgeo.2012.01.004, 2012a.

Chapligin, B., Meyer, H., Swann, G. E. A., Meyer-Jacob, C., and Hubberten, H.-W.: A 250 ka oxygen isotope record from diatoms at Lake El'gygytgyn, far east Russian Arctic, Clim. Past, 8, 1621–1636, https://doi.org/10.5194/cp-8-1621-2012, 2012b.

Chapligin, B., Meyer, H., Langer, M., and Hubberten, H.-W.: A 250 ka oxygen isotope record from diatoms and investigation of "super-interglacial" conditions during MIS 11 at Lake El'gygytgyn, Far East Russian Arctic, AGU Fall Meeting 2012, 3–7 December 2012, San Francisco, USA, 2012c.

Chapligin, B., Narancic, B., Meyer, H., and Pienitz, R.: Paleoenvironmental gateways in the eastern Canadian arctic – Recent isotope hydrology and diatom oxygen isotopes from Nettilling Lake, Baffin Island, Canada, Quaternary Sci. Rev., 147, 379–390, https://doi.org/10.1016/j.quascirev.2016.03.028, 2016a.

Chapligin, B., Narancic, B., Meyer, H., and Pienitz, R.: Paleoenvironmental gateways in the eastern Canadian arctic – Recent isotope hydrology and diatom oxygen isotopes from Nettilling Lake, Baffin Island, Canada, Quaternary Sci. Rev., 147, 379–390, https://doi.org/10.1016/j.quascirev.2016.03.028, 2016b.

Chondrogianni, C., Ariztegui, D., Rolph, T., Juggins, S., Shemesh, A., Rietti-Shati, M., Niessen, F., Guilizzoni, P., Lami, A., McKenzie, J. A., and Oldfield, F.: Millennial to interannual climate variability in the Mediterranean during the Last Glacial Maximum, Quatern. Int., 122, 31–41, https://doi.org/10.1016/j.quaint.2004.01.029, 2004.

Danek, C., Gierz, P., Kostrova, S. S., Meister, P., Meyer, H., and Werner, M.: Eurasian Holocene climate trends in transient coupled climate simulations and stable oxygen isotope records, J. Quaternary Sci., 37, 729–744, https://doi.org/10.1002/jqs.3396, 2021.

Dansgaard, W.: Stable isotopes in precipitation, Tellus, 16, 436–468, https://doi.org/10.1111/j.2153-3490.1964.tb00181.x, 1964.

Dean, J. R., Jones, M. D., Leng, M. J., Metcalfe, S. E., Sloane, H. J., Eastwood, W. J., and Roberts, C. N.: Seasonality of Holocene hydroclimate in the Eastern Mediterranean reconstructed using the oxygen isotope composition of carbonates and diatoms from Lake Nar, central Turkey, Holocene, 28, 267–276, https://doi.org/10.1177/0959683617721326, 2018.

Dodd, J. P. and Sharp, Z. D.: A laser fluorination method for oxygen isotope analysis of biogenic silica and a new oxygen isotope calibration of modern diatoms in freshwater environments, Geochim. Cosmochim. Ac., 74, 1381–1390, https://doi.org/10.1016/j.gca.2009.11.023, 2010.

Downing, J. A. and Duarte, C. M.: Abundance and size distribution of lakes, ponds and impoundments, in: Encyclopedia of Inland Waters, edited by: Likens, G. E., Elsevier, Oxford, UK, 469–478, https://doi.org/10.1016/B978-012370626-3.00025-9, 2009.

Harding, P., Bezrukova, E. V., Kostrova, S. S., Lacey, J. H., Leng, M. J., Meyer, H., Pavlova, L. A., Shchetnikov, A., Shtenberg, M. V., Tarasov, P. E., and Mackay, A. W.: Hydrological (in)stability in Southern Siberia during the Younger Dryas and early Holocene, Global Planet. Change, 195, https://doi.org/10.1016/j.gloplacha.2020.103333, 2020.

Helama, S., Jones, P. D., and Briffa, K. R.: Dark Ages Cold Period: A literature review and directions for future research, Holocene, 27, 1600–1606, https://doi.org/10.1177/0959683617693898, 2017.

Hernandez, A., Bao, R., Giralt, S., Leng, M. J., Barker, P. A., Saez, A., Pueyo, J. J., Moreno, A., Valero-Garces, B. L., and Sloane, H. J.: The palaeohydrological evolution of Lago Chungara (Andean Altiplano, northern Chile) during the Lateglacial and early Holocene using oxygen isotopes in diatom silica, J. Quaternary Sci., 23, 351–363, https://doi.org/10.1002/jqs.1173, 2008.

Hernandez, A., Giralt, S., Bao, R., Saez, A., Leng, M. J., and Barker, P. A.: ENSO and solar activity signals from oxygen isotopes in diatom silica during late glacial-Holocene transition in Central Andes (18° S), J. Paleolimnol., 44, 413–429, https://doi.org/10.1007/s10933-010-9412-x, 2010.

Hernandez, A., Bao, R., Giralt, S., Barker, P. A., Leng, M. J., Sloane, H. J., and Saez, A.: Biogeochemical processes controlling oxygen and carbon isotopes of diatom silica in Late Glacial to Holocene lacustrine rhythmites, Palaeogeogr. Palaeocl., 299, 413–425, https://doi.org/10.1016/j.palaeo.2010.11.020, 2011.

Hernandez, A., Bao, R., Giralt, S., Saez, A., Leng, M. J., Barker, P. A., Kendrick, C. P., and Sloane, H. J.: Climate, catchment runoff and limnological drivers of carbon and oxygen isotope composition of diatom frustules from the central Andean Altiplano during the Lateglacial and Early Holocene, Quaternary Sci. Rev., 66, 64–73, https://doi.org/10.1016/j.quascirev.2012.10.013, 2013.

Herzschuh, U., Birks, H. J. B., Laepple, T., Andreev, A., Melles, M., and Brigham-Grette, J.: Glacial legacies on interglacial vegetation at the Pliocene-Pleistocene transition in NE Asia, Nat. Commun., 7, 11967, https://doi.org/10.1038/ncomms11967, 2016.

Herzschuh, U., Böhmer, T., Li, C., and Cao, X.: Northern Hemisphere temperature and precipitation reconstruction from taxonomically harmonized pollen data set with revised chronologies using WA-PLS and MAT (LegacyClimate 1.0), PANGAEA [dataset], https://doi.org/10.1594/PANGAEA.930512, 2021.

Herzschuh, U., Böhmer, T., Li, C., Chevalier, M., Hébert, R., Dallmeyer, A., Cao, X., Bigelow, N. H., Nazarova, L., Novenko, E. Y., Park, J., Peyron, O., Rudaya, N. A., Schlütz, F., Shumilovskikh, L. S., Tarasov, P. E., Wang, Y., Wen, R., Xu, Q., and Zheng, Z.: LegacyClimate 1.0: a dataset of pollen-based climate reconstructions from 2594 Northern Hemisphere sites covering the last 30 kyr and beyond, Earth Syst. Sci. Data, 15, 2235–2258, https://doi.org/10.5194/essd-15-2235-2023, 2023a.

Herzschuh, U., Böhmer, T., Chevalier, M., Hébert, R., Dallmeyer, A., Li, C., Cao, X., Peyron, O., Nazarova, L., Novenko, E. Y., Park, J., Rudaya, N. A., Schlütz, F., Shumilovskikh, L. S., Tarasov, P. E., Wang, Y., Wen, R., Xu, Q., and Zheng, Z.: Regional pollen-based Holocene temperature and precipitation patterns depart from the Northern Hemisphere mean trends, Clim. Past, 19, 1481–1506, https://doi.org/10.5194/cp-19-1481-2023, 2023b.

Heyng, A. M., Mayr, C., Lücke, A., Moschen, R., Wissel, H., Striewski, B., and Bauersachs, T.: Middle and Late Holocene paleotemperatures reconstructed from oxygen isotopes and GDGTs of sediments from Lake Pupuke, New Zealand, Quatern. Int., 374, 3–14, https://doi.org/10.1016/j.quaint.2014.12.040, 2015.

Hu, F. S. and Shemesh, A.: A biogenic-silica δ^{18}O record of climatic change during the last glacial–interglacial transition in southwestern Alaska, Quaternary Res., 59, 379–385, https://doi.org/10.1016/s0033-5894(03)00056-5, 2003.

Hu, F. S., Kaufman, D., Yoneji, S., Nelson, D., Shemesh, A., Huang, Y., Tian, J., Bond, G., Clegg, B., and Brown, T.: Cyclic Variation and Solar Forcing of Holocene Climate in the Alaskan Subarctic, Science, 301, 1890–1893, https://doi.org/10.1126/science.1088568, 2003.

IAEA/WMO: Global Network of Isotopes in Precipitation, The GNIP Database, https://nucleus.iaea.org/wiser/index.aspx (last access: August 2022), 2022.

Jones, V. J., Leng, M. J., Solovieva, N., Sloane, H. J., and Tarasov, P.: Holocene climate of the Kola Peninsula; evidence from the oxygen isotope record of diatom silica, Quaternary Sci. Rev., 23, 833–839, https://doi.org/10.1016/j.quascirev.2003.06.014, 2004.

Jonsson, C. E., Rosqvist, G. C., Leng, M. J., Bigler, C., Bergman, J., Tillman, P. K., and Sloane, H. J.: High-resolution diatom δ^{18}O records, from the last 150 years, reflecting changes in amount of winter precipitation in two sub-Arctic high-altitude lakes in the Swedish Scandes, J. Quaternary Sci., 25, 918–930, https://doi.org/10.1002/jqs.1372, 2010.

Kalmychkov, G., Kuz'min, M., Pokrovskii or Pokrovsky, B., and Kostrova, S.: Oxygen isotopic composition in diatom algae frustules from Lake Baikal sediments: Annual mean temperature variations during the last 40 Ka, Dokl. Earth Sci., 413, 206–209, https://doi.org/10.1134/S1028334X07020158, 2007.

Kaufman, D., McKay, N., Routson, C., Erb, M., Dätwyler, C., Sommer, P. S., Heiri, O., and Davis, B.: Holocene global mean surface temperature, a multi-method reconstruction approach, Scientific Data, 7, 201, https://doi.org/10.1038/s41597-020-0530-7, 2020.

Kaufman, D. S. and Broadman, E.: Revisiting the Holocene global temperature conundrum, Nature, 614, 425–435, https://doi.org/10.1038/s41586-022-05536-w, 2023.

Kaufman, D. S., Ager, T. A., Anderson, N. J., Anderson, P. M., Andrews, J. T., Bartlein, P. J., Brubaker, L. B., Coats, L. L., Cwynar, L. C., Duvall, M. L., Dyke, A. S., Edwards, M. E., Eisner, W. R., Gajewski, K., Geirsdóttir, A., Hu, F. S., Jennings, A. E., Kaplan, M. R., Kerwin, M. W., Lozhkin, A. V., MacDonald, G. M., Miller, G. H., Mock, C. J., Oswald, W. W., Otto-Bliesner, B. L., Porinchu, D. F., Rühland, K., Smol, J. P., Steig, E. J., and Wolfe, B. B.: Holocene thermal maximum in the western Arctic (0–180° W), Quaternary Sci. Rev., 23, 529–560, https://doi.org/10.1016/j.quascirev.2003.09.007, 2004.

Konecky, B. L., McKay, N. P., Churakova (Sidorova), O. V., Comas-Bru, L., Dassié, E. P., DeLong, K. L., Falster, G. M., Fischer, M. J., Jones, M. D., Jonkers, L., Kaufman, D. S., Leduc, G., Managave, S. R., Martrat, B., Opel, T., Orsi, A. J., Partin, J. W., Sayani, H. R., Thomas, E. K., Thompson, D. M., Tyler, J. J., Abram, N. J., Atwood, A. R., Cartapanis, O., Conroy, J. L., Curran, M. A., Dee, S. G., Deininger, M., Divine, D. V., Kern, Z., Porter, T. J., Stevenson, S. L., von Gunten, L., and Iso2k Project Members:

The Iso2k database: a global compilation of paleo-$\delta^{18}O$ and $\delta^{2}H$ records to aid understanding of Common Era climate, Earth Syst. Sci. Data, 12, 2261–2288, https://doi.org/10.5194/essd-12-2261-2020, 2020.

Kostrova, S. S., Meyer, H., Chapligin, B., Bezrukova, E. V., Tarasov, P. E., and Kuz'min, M. I.: Reconstruction of the Holocene climate of Transbaikalia: Evidence from the oxygen isotope analysis of fossil diatoms from Kotokel Lake, Dokl. Earth Sci., 451, 732–736, https://doi.org/10.1134/S1028334x13070039, 2013a.

Kostrova, S. S., Meyer, H., Chapligin, B., Kossler, A., Bezrukova, E. V., and Tarasov, P. E.: Holocene oxygen isotope record of diatoms from Lake Kotokel (southern Siberia, Russia) and its palaeoclimatic implications, Quatern. Int., 290, 21–34, https://doi.org/10.1016/j.quaint.2012.05.011, 2013b.

Kostrova, S. S., Meyer, H., Chapligin, B., Tarasov, P. E., and Bezrukova, E. V.: The last glacial maximum and late glacial environmental and climate dynamics in the Baikal region inferred from an oxygen isotope record of lacustrine diatom silica, Quatern. Int., 348, 25–36, https://doi.org/10.1016/j.quaint.2014.07.034, 2014.

Kostrova, S. S., Meyer, H., Tarasov, P. E., Bezrukova, E. V., Chapligin, B., Kossler, A., Pavlova, L. A., and Kuzmin, M. I.: Oxygen isotope composition of diatoms from sediments of Lake Kotokel (Buryatia), Russ. Geol. Geophys.+, 57, 1239–1247, https://doi.org/10.1016/j.rgg.2016.08.009, 2016.

Kostrova, S. S., Meyer, H., Bailey, H. L., Ludikova, A. V., Gromig, R., Kuhn, G., Shibaev, Y. A., Kozachek, A. V., Ekaykin, A. A., and Chapligin, B.: Holocene hydrological variability of Lake Ladoga, northwest Russia, as inferred from diatom oxygen isotopes, Boreas, 48, 361–376, https://doi.org/10.1111/bor.12385, 2019.

Kostrova, S. S., Biskaborn, B. K., Pestryakova, L. A., Fernandoy, F., Lenz, M. M., and Meyer, H.: Climate and environmental changes of the Lateglacial transition and Holocene in northeastern Siberia: Evidence from diatom oxygen isotopes and assemblage composition at Lake Emanda, Quaternary Sci. Rev., 259, 106905, https://doi.org/10.1016/j.quascirev.2021.106905, 2021.

Koutsodendris, A., Pross, J., Müller, U. C., Brauer, A., Fletcher, W. J., Kühl, N., Kirilova, E., Verhagen, F. T. M., Lücke, A., and Lotter, A. F.: A short-term climate oscillation during the Holsteinian interglacial (MIS 11c): An analogy to the 8.2 ka climatic event?, Global Planet. Change, 92–93, 224–235, https://doi.org/10.1016/j.gloplacha.2012.05.011, 2012.

Kwiecien, O., Stockhecke, M., Pickarski, N., Heumann, G., Litt, T., Sturm, M., Anselmetti, F., Kipfer, R., and Haug, G. H.: Dynamics of the last four glacial terminations recorded in Lake Van, Turkey, Quaternary Sci. Rev., 104, 42–52, https://doi.org/10.1016/j.quascirev.2014.07.001, 2014.

Lamb, A. L., Leng, M. J., Sloane, H. J., and Telford, R. J.: A comparison of the palaeoclimate signals from diatom oxygen isotope ratios and carbonate oxygen isotope ratios from a low latitude crater lake, Palaeogeogr. Palaeocl., 223, 290–302, https://doi.org/10.1016/j.palaeo.2005.04.011, 2005.

Lasher, G., Axford, Y., McFarlin, J., Kelly, M., Osterberg, E., and Berkelhammer, M.: Holocene temperatures and isotopes of precipitation in Northwest Greenland recorded in lacustrine organic materials, Quaternary Sci. Rev., 170, 45–55, https://doi.org/10.1016/j.quascirev.2017.06.016, 2017.

Laskar, J., Robutel, P., Joutel, F., Gastineau, M., Correia, A. C. M., and Levrard, B.: A long-term numerical solution for the insolation quantities of the Earth, Astron. Astrophys., 428, 261–285, 2004.

Leclerc, A. J. and Labeyrie, L.: Temperature dependence of the oxygen isotopic fractionation between diatom silica and water, Earth Planet. Sc. Lett., 84, 69–74, https://doi.org/10.1016/0012-821X(87)90177-4, 1987.

Leng, M., Barker, P., Greenwood, P., Roberts, N., and Reed, J.: Oxygen isotope analysis of diatom silica and authigenic calcite from Lake Pinarbasi, Turkey, J. Paleolimnol., 25, 343–349, https://doi.org/10.1023/A:1011169832093, 2001.

Leng, M. J. (Ed.): Isotopes in palaeoenvironmental research, in: Developments in paleoenvironmental research, Vol. 10, xviii, Springer, Dordrecht, 307 pp., ISBN 13:9789048166749, 2006.

Leng, M. J. and Barker, P. A.: A review of the oxygen isotope composition of lacustrine diatom silica for palaeoclimate reconstruction, Earth-Sci. Rev., 75, 5–27, https://doi.org/10.1016/j.earscirev.2005.10.001, 2006.

Leng, M. J. and Marshall, J. D.: Palaeoclimate interpretation of stable isotope data from lake sediment archives, Quaternary Sci. Rev., 23, 811–831, https://doi.org/10.1016/j.quascirev.2003.06.012, 2004.

Leng, M. J., Metcalfe, S. E., and Davies, S. J.: Investigating late holocene climate variability in central mexico using carbon isotope ratios in organic materials and oxygen isotope ratios from diatom silica within lacustrine sediments, J. Paleolimnol., 34, 413–431, https://doi.org/10.1007/s10933-005-6748-8, 2005.

Lisiecki, L. E. and Raymo, M. E.: A Pliocene–Pleistocene stack of 57 globally distributed benthic $\delta^{18}O$ records, Paleoceanography, 20, PA1003, https://doi.org/10.1029/2004pa001071, 2005.

Liu, Z. , Zhu, J. , Rosenthal, Y. , Zhang, X. , Otto-Bliesner, B. L. , Timmermann, A. , Smith, R. S. , Lohmann, G. , Zheng, W., and Timm, O. E.: The Holocene temperature conundrum, P. Natl. Acad. Sci. USA, 111, E3501–E3505, https://doi.org/10.1073/pnas.1407229111, 2014.

Ljungqvist, F. C.: A new reconstruction of temperature variability in the extra-tropical Northern Hemisphere during the last two millennia, Geogr. Ann.-A,, 92, 339–351, https://doi.org/10.1111/j.1468-0459.2010.00399.x, 2010.

Mackay, A. W., Karabanov, E., Leng, M. J., Sloane, H. J., Morley, D. W., Panizzo, V. N., Khursevich, G., and Williams, D.: Reconstructing hydrological variability in Lake Baikal during MIS 11: an application of oxygen isotope analysis of diatom silica, J. Quaternary Sci., 23, 365–374, https://doi.org/10.1002/jqs.1174, 2008.

Mackay, A. W., Swann, G. E. A., Brewer, T. S., Leng, M. J., Morley, D. W., Piotrowska, N., Rioual, P., and White, D.: A reassessment of late glacial – Holocene diatom oxygen isotope record from Lake Baikal using a geochemical mass-balance approach, J. Quaternary Sci., 26, 627–634, https://doi.org/10.1002/jqs.1484, 2011.

Mackay, A. W., Swann, G. E. A., Fagel, N., Fietz, S., Leng, M. J., Morley, D., Rioual, P., and Tarasov, P.: Hydrological instability during the Last Interglacial in central Asia: a new diatom oxygen isotope record from Lake Baikal, Quaternary Sci. Rev., 66, 45–54, https://doi.org/10.1016/j.quascirev.2012.09.025, 2013.

Magyari, E. K., Demeny, A., Buczko, K., Kern, Z., Vennemann, T., Forizs, I., Vincze, I., Braun, M., Kovacs, J. I.,

Udvardi, B., and Veres, D.: A 13,600-year diatom oxygen isotope record from the South Carpathians (Romania): Reflection of winter conditions and possible links with North Atlantic circulation changes, Quatern. Int., 293, 136–149, https://doi.org/10.1016/j.quaint.2012.05.042, 2013.

Mann, M. E., Zhang, Z., Rutherford, S., Bradley, R. S., Hughes, M. K., Shindell, D., Ammann, C., Faluvegi, G., and Ni, F.: Global Signatures and Dynamical Origins of the Little Ice Age and Medieval Climate Anomaly, Science, 326, 1256–1260, https://doi.org/10.1126/science.1177303, 2009.

Marcott, S., Shakun, J., Clark, P., and Mix, A.: A Reconstruction of Regional and Global Temperature for the Past 11,300 Years, Science, 339, 1198–1201, https://doi.org/10.1126/science.1228026, 2013.

Matheney, R. K. and Knauth, L. P.: Oxygen-isotope fractionation between marine biogenic silica and seawater, Geochim. Cosmochim. Ac., 53, 3207–3214, https://doi.org/10.1016/0016-7037(89)90101-4, 1989.

Matthews, J. A. and Briffa, K. R.: The 'Little Ice Age': Re-Evaluation of an Evolving Concept, Geogr. Ann.-A, 87, 17–36, 2005.

McKay, N. P., Kaufman, D. S., Routson, C. C., Erb, M. P., and Zander, P. D.: The onset and rate of Holocene Neoglacial cooling in the Arctic, Geophys. Res. Lett., 45, 12487–12496, https://doi.org/10.1029/2018GL079773, 2018.

Meister, P., Alexandre, A., Bailey, H., Barker, P., Biskaborn, B. K, Broadman, E., Cartier, R., Chapligin, B., Couapel, M. J. J, Dean, J. R, Diekmann, B., Harding, P., Henderson, A., Hernandez, A., Herzschuh, U., Kostrova, S. S., Lacey, J. H., Leng, M. J., Lücke, A., Mackay, A. W., Magyari, E. K., Narancic, B., Porchier, C., Rosqvist, G. C., Shemesh, A., Sonzogni, C., Swann, G. E. A., Sylvestre, F., and Meyer, H.: A global compilation of diatom silica oxygen isotope records from lake sediment, PANGAEA [data set], https://doi.pangaea.de/10.1594/PANGAEA.957160, 2024.

Melles, M., Brigham-Grette, J., Minyuk, P. S., Nowaczyk, N. R., Wennrich, V., DeConto, R. M., Anderson, P. M., Andreev, A. A., Coletti, A., Cook, T. L., Haltia-Hovi, E., Kukkonen, M., Lozhkin, A. V., Rosén, P., Tarasov, P., Vogel, H., and Wagner, B.: 2.8 Million Years of Arctic Climate Change from Lake El'gygytgyn, NE Russia, Science, 337, 315–320, https://doi.org/10.1126/science.1222135, 2012.

Messager, M. L., Lehner, B., Grill, G., Nedeva, I., and Schmitt, O.: Estimating the volume and age of water stored in global lakes using a geo-statistical approach, Nat. Commun., 7, 13603, https://doi.org/10.1038/ncomms13603, 2016.

Meyer, H., Chapligin, B., Hoff, U., Nazarova, L., and Diekmann, B.: Oxygen isotope composition of diatoms as Late Holocene climate proxy at Two-Yurts Lake, Central Kamchatka, Russia, Global Planet. Change, 134, 118–128, https://doi.org/10.1016/j.gloplacha.2014.04.008, 2015a.

Meyer, H., Opel, T., Laepple, T., Dereviagin, A. Y., Hoffmann, K., and Werner, M.: Long-term winter warming trend in the Siberian Arctic during the mid- to late Holocene, Nat. Geosci., 8, 122–125, https://doi.org/10.1038/ngeo2349, 2015b.

Meyer, H., Kostrova, S. S., Meister, P., Lenz, M. M., Kuhn, G., Nazarova, L., Syrykh, L. S., and Dvornikov, Y.: Lacustrine diatom oxygen isotopes as palaeo precipitation proxy – Holocene environmental and snowmelt variations recorded at Lake Bolshoye Shchuchye, Polar Urals, Russia, Quaternary Sci. Rev., 290, 107620, https://doi.org/10.1016/j.quascirev.2022.107620, 2022.

Morley, D. W., Leng, M. J., Mackay, A. W., Sloane, H. J., Rioual, P., and Battarbee, R. W.: Cleaning of lake sediment samples for diatom oxygen isotope analysis, J. Paleolimnol., 31, 391–401, https://doi.org/10.1023/B:JOPL.0000021854.70714.6b, 2004.

Morley, D. W., Leng, M. J., Mackay, A. W., and Sloane, H. J.: Late glacial and Holocene environmental change in the Lake Baikal region documented by oxygen isotopes from diatom silica, Global Planet. Change, 46, 221–233, https://doi.org/10.1016/j.gloplacha.2004.09.018, 2005.

Moschen, R., Lücke, A., and Schleser, G. H.: Sensitivity of biogenic silica oxygen isotopes to changes in surface water temperature and palaeoclimatology, Geophys. Res. Lett., 32, L07708, https://doi.org/10.1029/2004GL022167, 2005.

Narancic, B., Pienitz, R., Chapligin, B., Meyer, H., Francus, P., and Guilbault, J.-P.: Postglacial environmental succession of Nettilling Lake (Baffin Island, Canadian Arctic) inferred from biogeochemical and microfossil proxies, Quaternary Sci. Rev., 147, 391–405, https://doi.org/10.1016/j.quascirev.2015.12.022, 2016.

Neukom, R., Steiger, N., Gómez-Navarro, J. J., Wang, J., and Werner, J. P.: No evidence for globally coherent warm and cold periods over the preindustrial Common Era, Nature, 571, 550–554, https://doi.org/10.1038/s41586-019-1401-2, 2019.

Opel, T., Wetterich, S., Meyer, H., Dereviagin, A. Y., Fuchs, M. C., and Schirrmeister, L.: Ground-ice stable isotopes and cryostratigraphy reflect late Quaternary palaeoclimate in the Northeast Siberian Arctic (Oyogos Yar coast, Dmitry Laptev Strait), Clim. Past, 13, 587–611, https://doi.org/10.5194/cp-13-587-2017, 2017.

Patton, H., Hubbard, A., Andreassen, K., Winsborrow, M., and Stroeven, A. P.: The build-up, configuration, and dynamical sensitivity of the Eurasian ice-sheet complex to Late Weichselian climatic and oceanic forcing, Quaternary Sci. Rev., 153, 97–121, https://doi.org/10.1016/j.quascirev.2016.10.009, 2016.

Pfalz, G., Diekmann, B., Freytag, J.-C., and Biskaborn, B. K.: Harmonizing heterogeneous multi-proxy data from lake systems, Comput. Geosci., 153, 104791, https://doi.org/10.1016/j.cageo.2021.104791, 2021.

Polissar, P., Abbott, M., Shemesh, A., Wolfe, A., and Bradley, R.: Holocene hydrologic balance of tropical South America from oxygen isotopes of lake sediment opal, Venezuelan Andes, Earth Planet. Sc. Lett., 242, 375–389, https://doi.org/10.1016/j.epsl.2005.12.024, 2006.

Quesada, B., Sylvestre, F., Vimeux, F., Black, J., Paillès, C., Sonzogni, C., Alexandre, A., Blard, P.-H., Tonetto, A., Mazur, J.-C., and Bruneton, H.: Impact of Bolivian paleolake evaporation on the $\delta^{18}O$ of the Andean glaciers during the last deglaciation (18.5–11.7 ka): diatom-inferred $\delta^{18}O$ values and hydro-isotopic modeling, Quaternary Sci. Rev., 120, 93–106, https://doi.org/10.1016/j.quascirev.2015.04.022, 2015.

Renssen, H., Seppä, H., Heiri, O., Roche, D. M., Goosse, H., and Fichefet, T.: The spatial and temporal complexity of the Holocene thermal maximum, Nat. Geosci., 2, 411–414, https://doi.org/10.1038/ngeo513, 2009.

Richter, F. M. and Turekian, K. K.: Simple models for the geochemical response of the ocean to climatic and tectonic forcing, Earth Planet. Sc. Lett., 119, 121–131, https://doi.org/10.1016/0012-821X(93)90010-7, 1993.

Rietti-Shati, M., Shemesh, A., and Karlen, W.: A 3000-Year Climatic Record from Biogenic Silica Oxygen Isotopes in an Equatorial High-Altitude Lake, Science, 281, 980–982, https://doi.org/10.1126/science.281.5379.980, 1998.

Rosqvist, G., Rietti-Shati, M., and Shemesh, A.: Late Glacial to middle Holocene climatic record of lacustrine biogenic silica oxygen isotopes from a Southern Ocean Island, Geology, 27, https://doi.org/10.1130/0091-7613(1999)027<0967:LGTMHC>2.3.CO;2, 1999.

Rosqvist, G., Jonsson, C., Yam, R., Karlen, W., and Shemesh, A.: Diatom oxygen isotopes in pro-glacial lake sediments from northern Sweden: a 5000 year record of atmospheric circulation, Quaternary Sci. Rev., 23, 851–859, https://doi.org/10.1016/j.quascirev.2003.06.009, 2004.

Rosqvist, G. C., Leng, M. J., Goslar, T., Sloane, H. J., Bigler, C., Cunningham, L., Dadal, A., Bergman, J., Berntsson, A., Jonsson, C., and Wastegård, S.: Shifts in precipitation during the last millennium in northern Scandinavia from lacustrine isotope records, Quaternary Sci. Rev., 66, 22–34, https://doi.org/10.1016/j.quascirev.2012.10.030, 2013.

Rozanski, K., Klisch, M. A., Wachniew, P., Gorczyca, Z., Goslar, T., Edwards, T. W. D., and Shemesh, A.: Oxygen-isotope geothermometers in lacustrine sediments: New insights through combined $\delta^{18}O$ analyses of aquatic cellulose, authigenic calcite and biogenic silica in Lake Gościąż, central Poland, Geochim. Cosmochim. Ac., 74, 2957–2969, https://doi.org/10.1016/j.gca.2010.02.026, 2010.

Ryves, D. B., Leng, M. J., Barker, P. A., Snelling, A. M., Sloane, H. J., Arrowsmith, C., Tyler, J. J., Scott, D. R., Radbourne, A. D., and Anderson, N. J.: Understanding the transfer of contemporary temperature signals into lake sediments via paired oxygen isotope ratios in carbonates and diatom silica: Problems and potential, Chem. Geol., 552, 119705, https://doi.org/10.1016/j.chemgeo.2020.119705, 2020.

Schiff, C., Kaufman, D., Wolfe, A., Dodd, J., and Sharp, Z.: Late Holocene storm-trajectory changes inferred from the oxygen isotope composition of lake diatoms, south Alaska, J. Paleolimnol., 41, 189–208, https://doi.org/10.1007/s10933-008-9261-z, 2009.

Schmidt, M., Fuchs, M., Henderson, A. C. G., Kossler, A., Leng, M. J., Mackay, A. W., Shemang, E., and Riedel, F.: Paleolimnological features of a mega-lake phase in the Makgadikgadi Basin (Kalahari, Botswana) during Marine Isotope Stage 5 inferred from diatoms, J. Paleolimnol., 58, 373–390, https://doi.org/10.1007/s10933-017-9984-9, 2017.

Shemesh, A. and Peteet, D.: Oxygen isotopes in fresh water biogenic opal – Northeastern US Alleröd-Younger Dryas temperature shift, Geophys. Res. Lett., 25, 1935–1938, https://doi.org/10.1029/98gl01443, 1998.

Shemesh, A., Rosqvist, G., Rietti-Shati, M., Rubensdotter, L., Bigler, C., Yam, R., and Karlén, W.: Holocene climatic change in Swedish Lapland inferred from an oxygen-isotope record of lacustrine biogenic silica, Holocene, 11, 447–454, https://doi.org/10.1191/095968301678302887, 2001a.

Shemesh, A., Rietti-Shati, M., Rioual, P., Battarbee, R., de Beaulieu, J.-L., Reille, M., Andrieu-Ponel, V., and Svitavská-Svobodová, H.: An oxygen isotope record of lacustrine opal from a European Maar indicates climatic stability during the Last Interglacial, Geophys. Res. Lett., 28, 2305–2308, https://doi.org/10.1029/2000GL012720, 2001b.

Smith, A. C., Leng, M. J., Swann, G. E. A., Barker, P. A., Mackay, A. W., Ryves, D. B., Sloane, H. J., Chenery, S. R. N., and Hems, M.: An experiment to assess the effects of diatom dissolution on oxygen isotope ratios, Rapid Commun. Mass Sp., 30, 293–300, https://doi.org/10.1002/rcm.7446, 2016.

Spielhagen, R. F. and Mackensen, A.: Upper ocean variability off NE Greenland (79° N) since the last glacial maximum reconstructed from stable isotopes in planktic foraminifer morphotypes, Quaternary Sci. Rev., 265, 107070, https://doi.org/10.1016/j.quascirev.2021.107070, 2021.

Street-Perrott, F. A., Barker, P. A., Leng, M. J., Sloane, H. J., Wooller, M. J., Ficken, K. J., and Swain, D. L.: Towards an understanding of late Quaternary variations in the continental biogeochemical cycle of silicon: multi-isotope and sediment-flux data for Lake Rutundu, Mt Kenya, East Africa, since 38 ka BP, J. Quaternary Sci., 23, 375–387, https://doi.org/10.1002/jqs.1187, 2008.

Subetto, D. A., Nazarova, L. B., Pestryakova, L. A., Syrykh, L. S., Andronikov, A. V., Biskaborn, B., Diekmann, B., Kuznetsov, D. D., Sapelko, T. V., and Grekov, I. M.: Paleolimnological studies in Russian northern Eurasia: A review, Contemp. Probl. Ecol., 10, 327–335, https://doi.org/10.1134/S1995425517040102, 2017.

Swann, G. E. A., Leng, M. J., Juschus, O., Melles, M., Brigham-Grette, J., and Sloane, H. J.: A combined oxygen and silicon diatom isotope record of Late Quaternary change in Lake El'gygytgyn, North East Siberia, Quaternary Sci. Rev., 29, 774–786, https://doi.org/10.1016/j.quascirev.2009.11.024, 2010.

Swann, G. E. A., Mackay, A. W., Vologina, E., Jones, M. D., Panizzo, V. N., Leng, M. J., Sloane, H. J., Snelling, A. M., and Sturm, M.: Lake Baikal isotope records of Holocene Central Asian precipitation, Quaternary Sci. Rev., 189, 210–222, https://doi.org/10.1016/j.quascirev.2018.04.013, 2018.

Tyler, J. J., Sloane, H. J., Rickaby, R. E. M., Cox, E. J., and Leng, M. J.: Post-mortem oxygen isotope exchange within cultured diatom silica, Rapid Commun. Mass Sp., 31, 1749–1760, https://doi.org/10.1002/rcm.7954, 2017.

Vinther, B. M., Buchardt, S. L., Clausen, H. B., Dahl-Jensen, D., Johnsen, S. J., Fisher, D. A., Koerner, R. M., Raynaud, D., Lipenkov, V., Andersen, K. K., Blunier, T., Rasmussen, S. O., Steffensen, J. P., and Svensson, A. M.: Holocene thinning of the Greenland ice sheet, Nature, 461, 385–388, https://doi.org/10.1038/nature08355, 2009.

Vyse, S. A., Herzschuh, U., Andreev, A. A., Pestryakova, L. A., Diekmann, B., Armitage, S. J., and Biskaborn, B. K.: Geochemical and sedimentological responses of arctic glacial Lake Ilirney, chukotka (far east Russia) to palaeoenvironmental change since ∼ 51.8 ka BP, Quaternary Sci. Rev., 247, 106607, https://doi.org/10.1016/j.quascirev.2020.106607, 2020.

Wanner, H.: Late-Holocene: cooler or warmer?, Holocene, 31, 1501–1506, https://doi.org/10.1177/09596836211019106, 2021.

Wanner, H., Pfister, C., and Neukom, R.: The variable European Little Ice Age, Quaternary Sci. Rev., 287, 107531, https://doi.org/10.1016/j.quascirev.2022.107531, 2022.

Wilson, K. E., Leng M. J., and Mackay, A. W.: The use of multivariate statistics to resolve multiple contamination signals in the oxygen isotope analysis of biogenic silica, J. Quaternary Sci., 29, 641–649, https://doi.org/10.1002/jqs.2729, 2014a.

Wilson, K. E., Maslin, M. A., Leng, M. J., Kingston, J. D., Deino, A. L., Edgar, R. K., and Mackay, A. W.: East African lake evidence for Pliocene millennial-scale climate variability, Geology, 42, 955–958, https://doi.org/10.1130/g35915.1, 2014b.

Wolfe, B. B., Falcone, M. D., Clogg-Wright, K. P., Mongeon, C. L., Yi, Y., Brock, B. E., Amour, N. A. S., Mark, W. A., and Edwards, T. W. D.: Progress in isotope paleohydrology using lake sediment cellulose, J. Paleolimnol., 37, 221–231, https://doi.org/10.1007/s10933-006-9015-8, 2007.